ELSEVIER

Engineering Analysis with Boundary Elements 28 (2004) 685–709

ENGINEERING ANALYSIS *with* BOUNDARY ELEMENTS

www.elsevier.com/locate/enganabound

Applications of the dual integral formulation in conjunction with fast multipole method in large-scale problems for 2D exterior acoustics

J.T. Chen*, K.H. Chen

Department of Harbor and River Engineering, National Taiwan Ocean University, Keelung, Taiwan, ROC

Received 17 September 2002; revised 27 March 2003; accepted 1 April 2003

Abstract

In this paper, we solve the large-scale problem for exterior acoustics by employing the concept of fast multipole method (FMM) to accelerate the construction of influence matrix in the dual boundary element method (DBEM). By adopting the addition theorem, the four kernels in the dual formulation are expanded into degenerate kernels, which separate the field point and source point. The separable technique can promote the efficiency in determining the coefficients in a similar way of the fast Fourier transform over the Fourier transform. The source point matrices decomposed in the four influence matrices are similar to each other or only some combinations. There are many zeros or the same influence coefficients in the field point matrices decomposed in the four influence matrices, which can avoid calculating repeatedly the same terms. The separable technique reduces the number of floating-point operations from $O(N^2)$ to $O(N \log^a(N))$, where N is number of elements and a is a small constant independent of N. To speed up the convergence in constructing the influence matrix, the center of multipole is designed to locate on the center of local coordinate for each boundary element. This approach enhances convergence by collocating multipoles on each center of the source element. The singular and hypersingular integrals are transformed into the summability of divergent series and regular integrals. Finally, the FMM is shown to reduce CPU time and memory requirement thus enabling us apply BEM to solve for large-scale problems. Five moment FMM formulation was found to be sufficient for convergence. The results are compared well with those of FEM, conventional BEM and analytical solutions and it shows the accuracy and efficiency of the FMM when compared with the conventional BEM.

Keywords: Fast multipole method; Large-scale problem; Exterior acoustics; Dual boundary element method; Hypersingular equation; Divergent series

1. Introduction

The boundary element method, sometimes referred to as the boundary integral equation method, is now establishing a position as an actual alternative to the FEM in many fields of engineering. It is necessary to discretize the boundary only instead of the domain, which takes a fewer time for one-dimension reduction in mesh generation. The dual boundary element method (DBEM), or so-called the dual boundary integral equation method developed by Hong and Chen [16,20], is particularly suitable for the problems with a degenerate boundary. The dual formulation also plays important roles in some other problems, e.g. the corner problem [15], adaptive BEM [7,24], the spurious eigenvalue of interior problem [12,13], the fictitious frequency of exterior problem [6,10,11,21], and the degenerate scale problem [8,9].

There is considerable interest in many applications for the solution of Helmholtz equation, when the wave length is short or the wave number is large after comparing with the size of boundary, and it is so-called the large-scale problem such as the scattering of high frequency acoustics, Stokes flows, molecular dynamics and electromagnetic-wave problems. However, the applications of BEM were limited in small-scale problems [14,17,26,27,29,30,34,37]. For large-scale problems, we need to model such problems with a large number (N) of boundary elements to accurately represent the geometry and the solution variation which may not be solved using a desktop computer. The complexity proportional of the conventional BEM is N^2 and it is expensive in the large-scale problem, but the finite element method (FEM) is N because of its banded coefficient matrix [30]. Multi-domain approach [18] or approximate theories such as

* Corresponding author. Tel.: +886-2-2462-2192x6140/6177; fax: +886-2-2463-2375.

E-mail address: jtchen@mail.ntou.edu.tw (J.T. Chen).

0955-7997/03/$ - see front matter © 2003 Elsevier Ltd. All rights reserved.
doi:10.1016/S0955-7997(03)00122-X

the theories of plates and shells have been employed to solve the problem using the parallel computers. When the size of the influence matrix by using BEM is so large that its storage and solution by Gaussian elimination may cause problems for desktop computer. Thus, the size of influence matrix becomes the limiting factor that large-scale problems can be solved with a particular computer. BEM with iterative solvers has been employed to deal with the problem [25,38]. The major computational cost of the iterative methods lies in the matrix–vector multiplication. To improve the efficiency in numerical computation of the dual BEM, we will adopt the fast multipole method (FMM) to accelerate the speed of calculation. This is due to the large domain and full influence matrix, and it takes a lot of CPU time and memory space to obtain the influence matrix. To overcome the disadvantages, the FMM will be shown to reduce CPU time and memory requirement from exponential order to logarithmic order thus enabling us apply BEM to really solve for large-scale problems.

The FMM was initially introduced by Rokhlin [34]. Applications of FMM for BEM analysis have been used by many researchers in various fields of science and engineering [2,3,27–34,36,37]. We will adopt the concept of FMM to accelerate the calculation of influence matrix in the dual BEM. By adopting the addition theorem, the four kernels in the dual formulation are expanded into degenerate kernels where the field point and source point are separated. The separable technique can promote the efficiency in determining the coefficients as shown in Fig. 1, in a similar way of the fast Fourier transform (FFT) over the Fourier transform (FT). The source point matrices decomposed in the four influence matrices are similar to each other or only some combinations. There are many zeros or the same influence coefficients in the field point matrices decomposed in the four influence matrices. Therefore, we can avoid calculating repeatedly the same terms. The separable technique reduces the number of floating-point operations from $O((N)^2)$ to $O(N\log^a(N))$. To accelerate the convergence in constructing the influence matrix, the center of multipole is designed to locate on the center of each boundary element. The singular and hypersingular integrals are transformed into the summability of divergent series and regular integrals.

In this paper, the acoustic scattering of general structure with the Neumann's boundary condition will be considered. The Burton and Miller formulation by combining the dual boundary integral equations will be utilized to solve the exterior acoustic problems for all wave numbers in order to overcome the problem of fictitious frequency. Finally, the CPU time and memory requirement will be calculated using the FMM for the large-scale problem. The numerical results will be compared with those of conventional DBEM and analytical solutions.

2. Mathematical formulation

2.1. Helmholtz equation in exterior acoustics

Let $D \subset D^d$ be an unbounded region, where d is the number of space dimensions, d can be 1, 2 or 3. The boundary of the domain D, denoted by B, is internal and assumed piecewise smooth. The outward unit vector normal to B is denoted by n. We assume that the boundary, B, admits the partition [22,35]

$$B = B_g \cup B_h, \tag{1}$$

$$\varnothing = B_g \cap B_h, \tag{2}$$

where B_g is the essential boundary with specified potential and B_h is the natural boundary with specified normal derivative of potential. We intend to study the effects of small disturbance to a given background flow in such a region, under the usual assumptions that leads to the equations of acoustics. Harmonic analysis leads to a boundary-value problem for the Helmholtz equation (or reduced wave equation): Find u in the exterior domain, the spatial component for the acoustic pressure or velocity potential [22,35], such that

$$-\mathscr{L}u(x) = f, \qquad x \text{ in } D, \tag{3}$$

$$u(x) = g, \qquad x \text{ on } B_g, \tag{4}$$

$$\frac{\partial u(x)}{\partial n} = \mathrm{i}kh, \qquad x \text{ on } B_h, \tag{5}$$

$$\lim_{R\to\infty} R^{\frac{1}{2}(d-1)}\left(\frac{\partial u}{\partial R} - \mathrm{i}ku\right) = 0, \qquad R \text{ at infinity}, \tag{6}$$

where $\mathscr{L}u := \nabla^2 u + k^2 u$ is the Helmholtz operator, ∇^2 is the Laplacian operator and $k \geq 0$ is the wave number; and in particular $\partial u/\partial n := \nabla u \cdot \mathbf{n}$ is the normal flux and ∇ is the gradient operator; $\mathrm{i}^2 = -1$, R is the distance from the origin to the field point. In the linearized equations of motion, velocity gradients produce a compression of the acoustic medium and pressure gradients are related to acceleration. Thus, if the dependent variable is, e.g. the acoustic pressure, then the Neumann boundary condition Eq. (5) represents a prescribed velocity distribution on that portion of the wet surface, where h is proportional to the velocity and the presence of $\mathrm{i}k$ is a consequence of differentiation with respect to time. Neumann boundary conditions are therefore very common in physical situations that entail *radiation*, and in the model problems and demonstrative examples that are subsequently considered we emphasize boundary conditions of this type. It is noted that the analysis is valid for any combination of boundary conditions on the wet surface for the boundary-value problem Eqs. (3)–(6), and by no means is it limited to Neumann problems. For *scattering* problems, a fixed rigid object is represented by a homogeneous Neumann boundary condition, often referred to as a hard scatter. Conversely, the homogeneous Dirichlet boundary condition, an appropriate representation

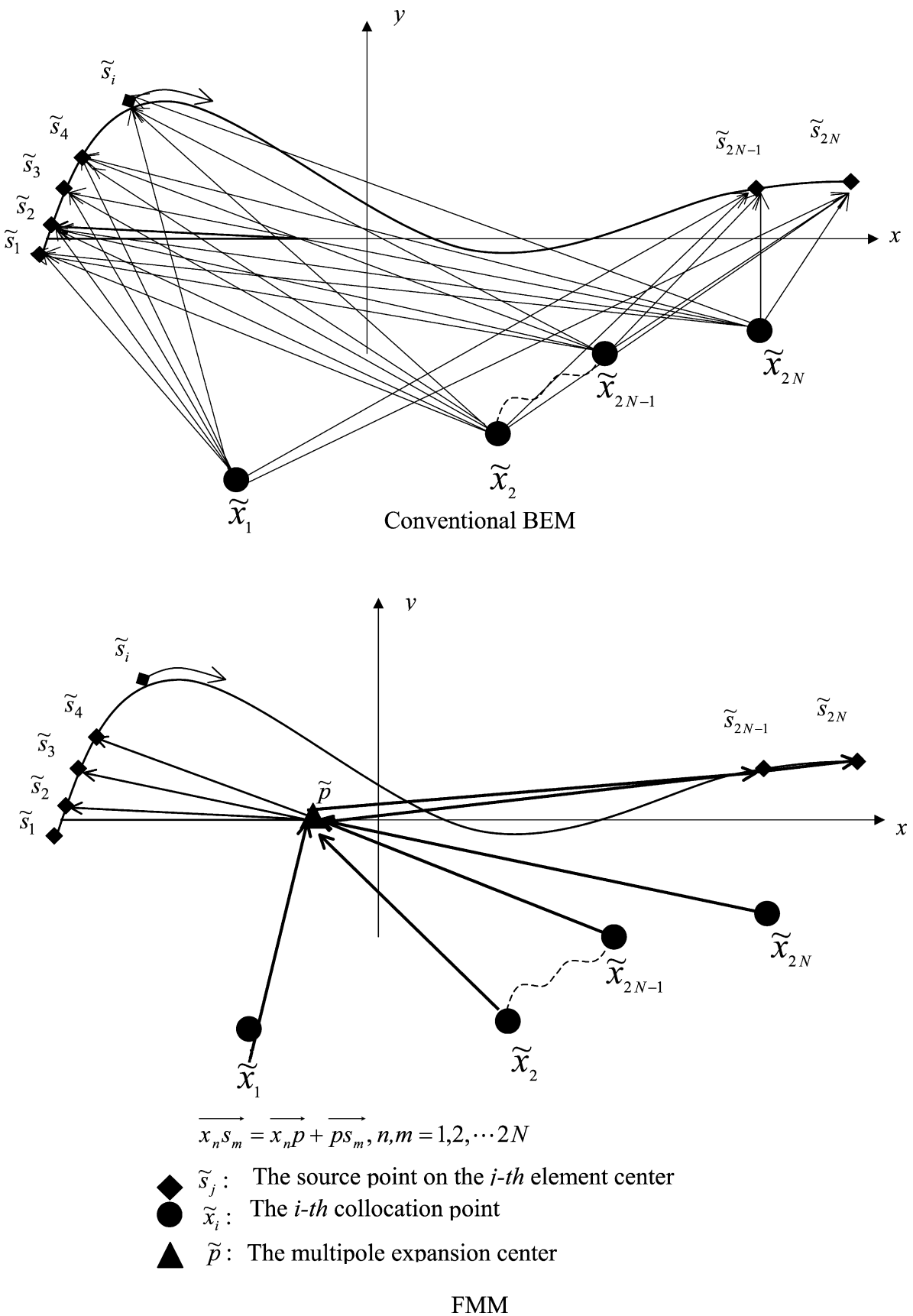

Fig. 1. Comparison of the scheme in the calculation of influence coefficients by using the conventional BEM and the FMM.

of a site of pressure release, is termed a soft scatter. An impedance boundary condition is a linear combination of the two [22,35].

The governing equation for an exterior acoustic problem is the Helmholtz equation as follows

$$(\nabla^2 + k^2)u(x_1, x_2) = 0, \qquad (x_1, x_2) \in D, \tag{7}$$

where f in Eq. (3) is zero (no sources), and k is the wave number, which is the angular frequency over the speed of sound. The boundary conditions can be either the Neumann or Dirichlet type.

Eq. (6) stems from the *Sommerfeld radiation condition* which allows only solutions with outgoing waves at infinity to be admitted. This boundary condition implies an integral form, the Rellich–Sommerfeld radiation condition

$$\int_{B_\infty} \left| \frac{\partial u}{\partial R} - iku \right|^2 \mathrm{d}B = 0, \tag{8}$$

where B_∞ is the surface of a sphere with an infinite radius. The radiation condition requires energy flux at infinity to be positive, thereby guaranteeing that the solution to the boundary-value problem in Eqs. (3)–(6) is unique. Appropriate representation of this condition is crucial to the reliability of any numerical formulation of the problem. In this section, the statement of problem follows the paper by Stewart and Hughes [35] since they present a typical formulation.

2.2. Dual boundary integral formulation

The first equation of the dual boundary integral equations for the domain point can be derived from the Green's third identity

$$2\pi u(\tilde{x}) = \int_B T(\tilde{s}, \tilde{x}) u(\tilde{s}) \mathrm{d}B(\tilde{s}) - \int_B U(\tilde{s}, \tilde{x}) \frac{\partial u(\tilde{s})}{\partial n_{\tilde{s}}} \mathrm{d}B(\tilde{s}), \quad \tilde{x} \in D, \tag{9}$$

where $\tilde{x}$ is the field point ($\tilde{x} = (x, y)$), $\tilde{s}$ is the source point, and

$$U(\tilde{s}, \tilde{x}) = -\frac{\pi \mathrm{i}}{2} H_0^{(1)}(k|\tilde{s} - \tilde{x}|), \tag{10}$$

in which $H_0^{(1)}(k|\tilde{s} - \tilde{x}|)$ is the first kind zeroth order Hankel function, and $T(\tilde{s}, \tilde{x})$ is defined by

$$T(\tilde{s}, \tilde{x}) \equiv \frac{\partial U(\tilde{s}, \tilde{x})}{\partial n_{\tilde{s}}}, \tag{11}$$

in which $n_{\tilde{s}}$ denotes the normal vector at the boundary point $\tilde{s}$, and $U(\tilde{s}, \tilde{x})$ is the fundamental solution which satisfies

$$\nabla^2 U(\tilde{x}, \tilde{s}) + k^2 U(\tilde{x}, \tilde{s}) = 2\pi\delta(\tilde{x} - \tilde{s}), \qquad \tilde{x} \in D. \tag{12}$$

In Eq. (12), $\delta(\tilde{x} - \tilde{s})$ is the Dirac-delta function. After taking normal derivative with respect to Eq. (9), the second equation of the dual boundary integral equations for the domain point is derived

$$2\pi \frac{\partial u(\tilde{x})}{\partial n_{\tilde{x}}} = \int_B M(\tilde{s}, \tilde{x}) u(\tilde{s}) \mathrm{d}B(\tilde{s}) - \int_B L(\tilde{s}, \tilde{x}) \frac{\partial u(\tilde{s})}{\partial n_{\tilde{s}}} \mathrm{d}B(\tilde{s}), \quad \tilde{x} \in D, \tag{13}$$

where

$$L(\tilde{s}, \tilde{x}) \equiv \frac{\partial U(\tilde{s}, \tilde{x})}{\partial n_{\tilde{x}}}, \tag{14}$$

$$M(\tilde{s}, \tilde{x}) \equiv \frac{\partial^2 U(\tilde{s}, \tilde{x})}{\partial n_{\tilde{x}} \, \partial n_{\tilde{s}}}, \tag{15}$$

in which $n_{\tilde{x}}$ represents the normal vector of $\tilde{x}$. The explicit forms for the four kernel functions are shown in Table 1. The boundary conditions can be either the Neumann or Dirichlet type. By moving the point x to the boundary, the dual equations for the boundary points are

$$\pi u(\tilde{x}) = \mathrm{CPV} \int_B T(\tilde{s}, \tilde{x}) u(\tilde{s}) \mathrm{d}B(\tilde{s}) - \mathrm{RPV} \int_B U(\tilde{s}, \tilde{x}) t(\tilde{s}) \mathrm{d}B(\tilde{s}), \quad \tilde{x} \in B, \tag{16}$$

Table 1
The properties of the kernel functions for the Helmhotz equation

Kernel $K(\tilde{s}, \tilde{x})$	$U(\tilde{s}, \tilde{x})$ $-\frac{i\pi H_0^{(1)}(\lambda r)}{2}$	$T(\tilde{s}, \tilde{x})$ $-\frac{i\lambda\pi}{2} H_1^{(1)}(\lambda r) \frac{y_i n_i}{r}$	$L(\tilde{s}, \tilde{x})$ $\frac{i\lambda\pi}{2} H_1^{(1)}(\lambda r) \frac{y_i \bar{n}_i}{r}$	$M(\tilde{s}, \tilde{x}) - \frac{i\lambda\pi}{2} \{\lambda \frac{H_2^{(1)}(\lambda r)}{r^2} y_i y_j n_i \bar{n}_j + \frac{H_1^{(1)}(\lambda r)}{r} n_i \bar{n}_i\}$
Order of singularity	$O(\ln r)$ weak	$O(1/r)$ strong	$O(1/r)$ strong	$O(1/r^2)$ hypersingular
Symmetry	$U(\tilde{s}, \tilde{x}) = U(\tilde{x}, \tilde{s})$	$T(\tilde{s}, \tilde{x}) = L(\tilde{x}, \tilde{s})$	$L(\tilde{s}, \tilde{x}) = T(\tilde{x}, \tilde{s})$	$M(\tilde{s}, \tilde{x}) = M(\tilde{x}, \tilde{s})$
Density function $v(\tilde{s})$	$\partial u/\partial n$	u	$\partial u/\partial n$	u
Potential type	Single layer	Double layer	Normal derivative of single layer	Normal derivative of double layer
$\int K(\tilde{s}, \tilde{x}) v(\tilde{s}) \mathrm{d}B(\tilde{s})$ continuity across boundary	Continuous	Discontinuous	Discontinuous	Psuedo-continuous
Jump value	No jump	$2\pi u$	$2\pi(\partial u/\partial n)$	No jump
Principal value	Riemann	Cauchy	Cauchy	Hadamard

Where $H_n^{(1)}(\lambda r)$ is first kind of the nth order Hankel function, $\bar{n}_i$ denotes the ith components of normal vector on $\bar{x}$, respectively.

$$\pi t(\tilde{x}) = \mathrm{HPV}\int_B M(\tilde{s},\tilde{x})u(\tilde{s})\mathrm{d}B(\tilde{s}) - \mathrm{CPV}\int_B L(\tilde{s},\tilde{x})t(\tilde{s})\mathrm{d}B(\tilde{s}), \quad \tilde{x}\in B, \tag{17}$$

where CPV, RPV and HPV denote the Cauchy principal value, the Riemann principal value and the Hadamard principal value, $t(\tilde{s}) = \partial u(\tilde{s})/\partial n_{\tilde{s}}$, B denotes the boundary enclosing D. The linear algebraic equations discretized from the dual boundary integral equations can be written as

$$[T]\{u\} = [U]\{t\}, \tag{18}$$
$$[M]\{u\} = [L]\{t\}, \tag{19}$$

where $\{u\}$ and $\{t\}$ are the boundary potential and flux, respectively. The influence coefficients of the four square matrices $[U]$, $[T]$, $[L]$ and $[M]$ can be represented as

$$U_{pq} = \mathrm{RPV}\int_{B_q} U(s_q,x_p)\mathrm{d}B(s_q), \tag{20}$$

$$T_{pq} = -\pi\delta_{pq} + \mathrm{CPV}\int_{B_q} T(s_q,x_p)\mathrm{d}B(s_q), \tag{21}$$

$$L_{pq} = \pi\delta_{pq} + \mathrm{CPV}\int_{B_q} L(s_q,x_p)\mathrm{d}B(s_q), \tag{22}$$

$$M_{pq} = \mathrm{HPV}\int_{B_q} M(s_q,x_p)\mathrm{d}B(s_q), \tag{23}$$

where the subscript p denotes the label on collocation point, B_q denotes the qth element and $\delta_{pq} = 1$ if $p = q$; otherwise it is zero. In order to overcome the problem of fictitious frequency, the Burton and Miller formulation [5] is employed by combining the dual equations as follows

$$\left\{[T] + \frac{i}{k}[M]\right\}\{u\} = \left\{[U] + \frac{i}{k}[L]\right\}\{t\}. \tag{24}$$

For all wave numbers, Eq. (24) can work well [4].

2.3. Expanding the four kernels using the multipole expansion method

By adopting the addition theorem, the four kernels in the dual formulation are expanded into degenerate kernels which separate the field point and source point [1]. The kernel function, $U(\tilde{s},\tilde{x})$, can be expanded into

$$U(\tilde{s},\tilde{x}) = \sum C_m(\tilde{x})R_m(\tilde{s}) = \begin{cases} U^i = -\dfrac{\pi\mathrm{i}}{2}\displaystyle\sum_{m=0}^{\infty}\varepsilon_m J_m(k|\tilde{x}-\tilde{p}|)H_m^{(1)}(k|\tilde{s}-\tilde{p}|)\cos(m\alpha), & |\tilde{s}-\tilde{p}| > |\tilde{x}-\tilde{p}|, \\ U^e = -\dfrac{\pi\mathrm{i}}{2}\displaystyle\sum_{m=0}^{\infty}\varepsilon_m H_m^{(1)}(k|\tilde{x}-\tilde{p}|)J_m(k|\tilde{s}-\tilde{p}|)\cos(m\alpha), & |\tilde{x}-\tilde{p}| > |\tilde{s}-\tilde{p}|, \end{cases} \tag{25}$$

where $\mathrm{i}^2 = -1$, $J_m(ks)$ is the first kind mth order Bessel function, $\tilde{p}$ is the center of multipole

$$\varepsilon_m = \begin{cases} 1, & m = 0 \\ 2, & m \neq 0 \end{cases}, \tag{26}$$

and

$$\alpha = \cos^{-1}\left(\frac{(\tilde{s}-\tilde{p})(\tilde{x}-\tilde{p})}{|(\tilde{s}-\tilde{p})||(\tilde{x}-\tilde{p})|}\right). \tag{27}$$

The definition sketch of the coordinate is shown in Fig. 2. The contour plot of potential for the U kernel can be shown in Fig. 3(a) for the series form using the degenerate kernel in Eq. (25) and Fig. 3(b) for the closed-form fundamental solution of Eq. (10). The kernel function, $T(\tilde{s},\tilde{x})$, can be expanded into

$$T(\tilde{s},\tilde{x}) = \sum_{m=0}^{\infty} C_m(\tilde{x})[\nabla R_m(\tilde{s})\cdot n_s] = \begin{cases} T^i = -\dfrac{\pi\mathrm{i}}{2}\displaystyle\sum_{m=0}^{\infty}\varepsilon_m J_m(k|\tilde{x}-\tilde{p}|)\left\{\frac{\partial H_m^{(1)}(k|\tilde{s}-\tilde{p}|)}{\partial n_s}\cos(m\alpha)\right. \\ \qquad \left. + H_m^{(1)}(k|\tilde{s}-\tilde{p}|)\dfrac{\partial\cos(m\alpha)}{\partial n_s}\right\}, \quad |\tilde{s}-\tilde{p}| > |\tilde{x}-\tilde{p}|, \\ T^e = -\dfrac{\pi\mathrm{i}}{2}\displaystyle\sum_{m=0}^{\infty}\varepsilon_m H_m^{(1)}(k|\tilde{x}-\tilde{p}|)\left\{\frac{\partial J_m(k|\tilde{s}-\tilde{p}|)}{\partial n_s}\right. \\ \qquad \left. \times\cos(m\alpha) + J_m(k|\tilde{s}-\tilde{p}|)\dfrac{\partial\cos(m\alpha)}{\partial n_s}\right\}, \\ \qquad |\tilde{x}-\tilde{p}| > |\tilde{s}-\tilde{p}|, \end{cases} \tag{28}$$

where

$$\frac{\partial J_m(k|\tilde{s}-\tilde{p}|)}{\partial n_s} = \frac{k}{2}[J_{m-1}(k|\tilde{s}-\tilde{p}|) - J_{m+1}(k|\tilde{s}-\tilde{p}|)] \times\frac{(s_i-p_i)n_i}{|\tilde{s}-\tilde{p}|}, \tag{29}$$

$$\frac{\partial H_m^{(1)}(k|\tilde{s}-\tilde{p}|)}{\partial n_{\tilde{s}}} = \frac{k}{2}[H_{m-1}^{(1)}(k|\tilde{s}-\tilde{p}|) - H_{m+1}^{(1)}(k|\tilde{s}-\tilde{p}|)] \times\frac{(s_i-p_i)n_i}{|\tilde{s}-\tilde{p}|}, \tag{30}$$

$$\frac{\partial\cos(m\alpha)}{\partial n_s} = -m\sin(m\alpha)(a_i n_i), \tag{31}$$

in which n_i is the ith component of the normal vector at $\tilde{s}$ and

$$a_1 = \frac{-1}{\sin(\alpha)}\frac{(s_2-p_2)^2(x_1-p_1) - (s_1-p_1)(s_2-p_2)(x_2-p_2)}{|\tilde{s}-\tilde{p}|^3|\tilde{x}-\tilde{p}|}, \tag{32}$$

$$a_2 = \frac{-1}{\sin(\alpha)}\frac{(s_1-p_1)^2(x_2-p_2) - (s_1-p_1)(s_2-p_2)(x_1-p_1)}{|\tilde{s}-\tilde{p}|^3|\tilde{x}-\tilde{p}|}, \tag{33}$$

By substituting Eqs. (29)–(31) into Eq. (28), we have

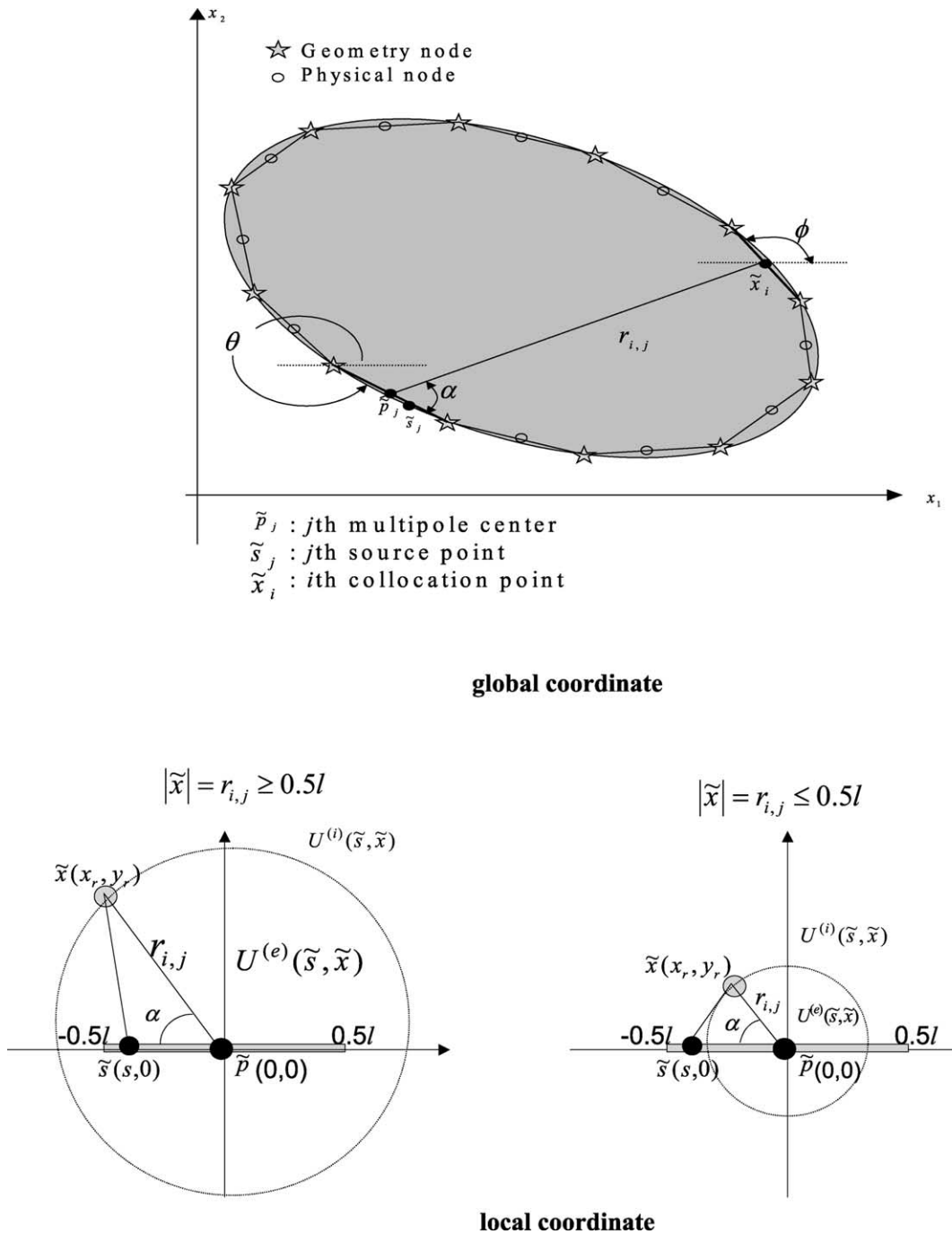

Fig. 2. The definition sketch of the coordinate, coordinate transformation and the position for the center of multipole.

$$T(\tilde{s},\tilde{x})\begin{cases} T^i = -\dfrac{\pi \mathrm{i}}{2}\displaystyle\sum_{m=0}^{\infty}\varepsilon_m J_m(k|\tilde{x}-\tilde{p}|)\Big\{\frac{k}{2}[H_{m-1}^{(1)}(k|\tilde{s}-\tilde{p}|)-H_{m+1}^{(1)}(k|\tilde{s}-\tilde{p}|)]\frac{(s_i-p_i)n_i}{|\tilde{s}-\tilde{p}|}\cos(m\alpha)+H_m^{(1)}(k|\tilde{s}-\tilde{p}|) \\ \qquad \times[-m\sin(m\alpha)(a_i n_i)]\Big\}, |\tilde{s}-\tilde{p}|>|\tilde{x}-\tilde{p}|, \\ T^e = -\dfrac{\pi \mathrm{i}}{2}\displaystyle\sum_{m=0}^{\infty}\varepsilon_m H_m^{(1)}(k|\tilde{x}-\tilde{p}|)\Big\{\frac{k}{2}[J_{m-1}(k|\tilde{s}-\tilde{p}|)-J_{m+1}(k|\tilde{s}-\tilde{p}|)]\frac{(s_i-p_i)n_i}{|\tilde{s}-\tilde{p}|}\cos(m\alpha)+J_m(k|\tilde{s}-\tilde{p}|) \\ \qquad \times[-m\sin(m\alpha)(a_i n_i)]\Big\}, |\tilde{x}-\tilde{p}|>|\tilde{s}-\tilde{p}|. \end{cases} \tag{34}$$

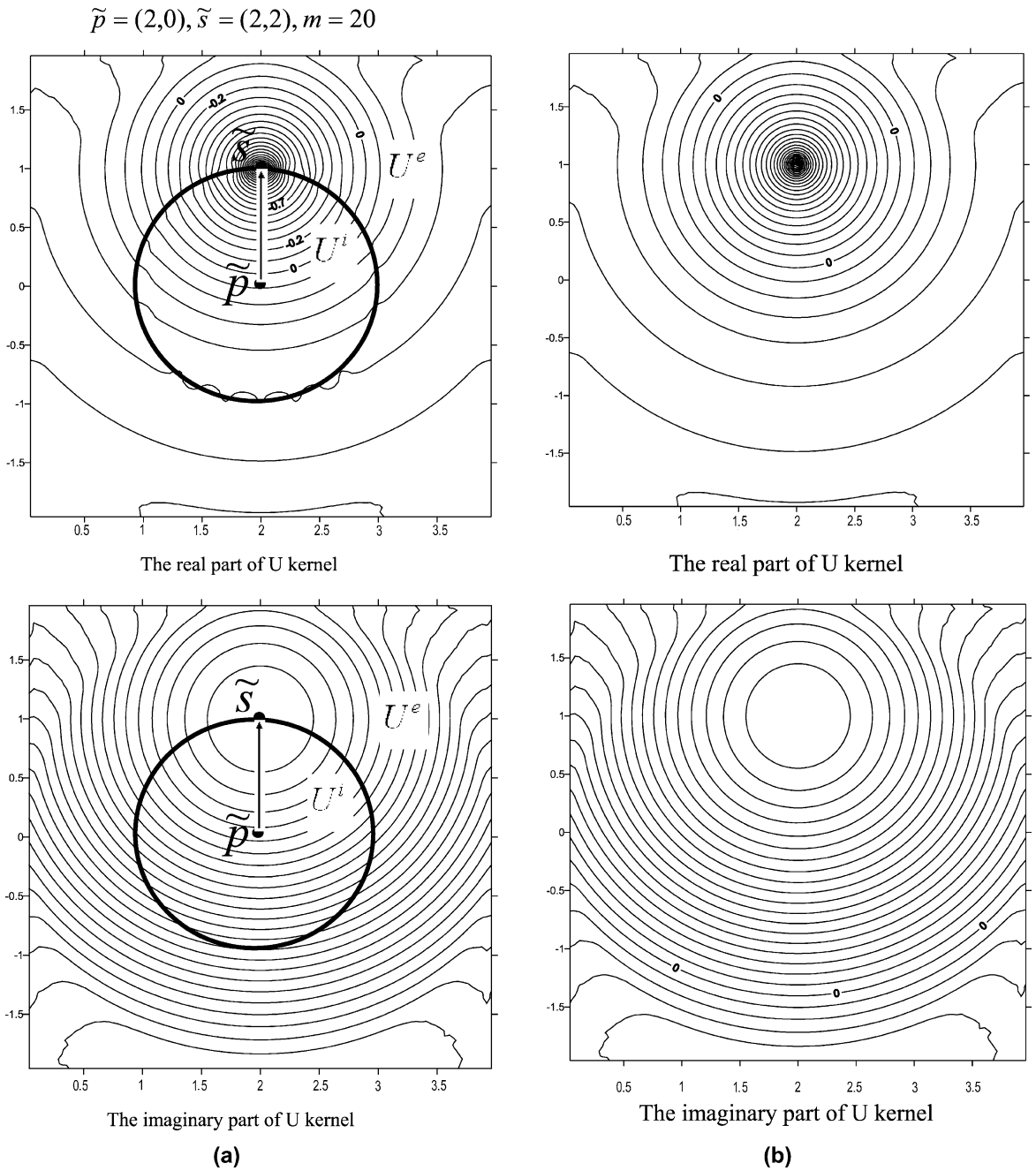

Fig. 3. The contour plot of potential for U kernel. (a) Degenerate kernel of Eq. (25), (b) Closed-form fundamental solution of Eq. (10).

The kernel function, $L(\tilde{s},\tilde{x})$, can be expanded into

$$L(\tilde{s},\tilde{x}) = \sum_{m=0}^{\infty} [\nabla C_m(\tilde{x})\cdot n_x] R_m(\tilde{s})$$

$$= \begin{cases} L^i = -\dfrac{\pi \mathrm{i}}{2} \displaystyle\sum_{m=0}^{\infty} \varepsilon_m H_m^{(1)}(k|\tilde{s}-\tilde{p}|)\left\{ \dfrac{\partial J_m(k|\tilde{x}-\tilde{p}|)}{\partial n_x}\cos(m\alpha) + J_m(k|\tilde{x}-\tilde{p}|)\dfrac{\partial \cos(m\alpha)}{\partial n_x} \right\}, & |\tilde{s}-\tilde{p}| > |\tilde{x}-\tilde{p}|, \\ L^e = -\dfrac{\pi \mathrm{i}}{2} \displaystyle\sum_{m=0}^{\infty} \varepsilon_m J_m(k|\tilde{s}-\tilde{p}|)\left\{ \dfrac{\partial H_m^{(1)}(k|\tilde{x}-\tilde{p}|)}{\partial n_x}\cos(m\alpha) + H_m^{(1)}(k|\tilde{x}-\tilde{p}|)\dfrac{\partial \cos(m\alpha)}{\partial n_x} \right\}, & |\tilde{x}-\tilde{p}| > |\tilde{s}-\tilde{p}|, \end{cases} \tag{35}$$

where

$$\frac{\partial J_m(k|\tilde{x}-\tilde{p}|)}{\partial n_x}=\frac{k}{2}[J_{m-1}(k|\tilde{x}-\tilde{p}|)-J_{m+1}(k|\tilde{x}-\tilde{p}|)]\frac{(x_i-p_i)\bar{n}_i}{|\tilde{x}-\tilde{p}|}, \tag{36}$$

$$\frac{\partial H_m^{(1)}(k|\tilde{x}-\tilde{p}|)}{\partial n_x}=\frac{k}{2}[H_{m-1}^{(1)}(k|\tilde{x}-\tilde{p}|)-H_{m+1}^{(1)}(k|\tilde{x}-\tilde{p}|)]\frac{(x_i-p_i)\bar{n}_i}{|\tilde{x}-\tilde{p}|}, \tag{37}$$

$$\frac{\partial \cos(m\alpha)}{\partial n_x}=-m\sin(m\alpha)(b_i\bar{n}_i), \tag{38}$$

in which $\bar{n}_i$ is the ith component of the normal vector at $\tilde{x}$ and

$$b_1=\frac{-1}{\sin(\alpha)}\frac{(s_1-p_1)(x_2-p_2)^2-(s_2-p_2)(x_1-p_1)(x_2-p_2)}{|\tilde{x}-\tilde{p}|^3|\tilde{s}-\tilde{p}|}, \tag{39}$$

$$b_2=\frac{-1}{\sin(\alpha)}\frac{(s_2-p_2)(x_1-p_1)^2-(s_1-p_1)(x_1-p_1)(x_2-p_2)}{|\tilde{x}-\tilde{p}|^3|\tilde{s}-\tilde{p}|}. \tag{40}$$

By substituting Eqs. (36)–(38) into Eq. (35), we have

$$L(\tilde{s},\tilde{x})\begin{cases} L^i=-\dfrac{\pi \mathrm{i}}{2}\displaystyle\sum_{m=0}^{\infty}\varepsilon_m H_m^{(1)}(k|\tilde{s}-\tilde{p}|)\Big\{\frac{k}{2}[J_{m-1}(k|\tilde{x}-\tilde{p}|)-J_{m+1}(k|\tilde{x}-\tilde{p}|)]\dfrac{(x_i-p_i)\bar{n}_i}{|\tilde{x}-\tilde{p}|}\cos(m\alpha)+J_m(k|\tilde{x}-\tilde{p}|) \\ \qquad \times[-m\sin(m\alpha)(b_i\bar{n}_i)]\Big\}, |\tilde{s}-\tilde{p}|>|\tilde{x}-\tilde{p}|, \\ L^e=-\dfrac{\pi \mathrm{i}}{2}\displaystyle\sum_{m=0}^{\infty}\varepsilon_m J_m(k|\tilde{s}-\tilde{p}|)\Big\{\frac{k}{2}[H_{m-1}^{(1)}(k|\tilde{x}-\tilde{p}|)-H_{m+1}^{(1)}(k|\tilde{x}-\tilde{p}|)]\dfrac{(x_i-p_i)\bar{n}_i}{|\tilde{x}-\tilde{p}|}\cos(m\alpha)+H_m^{(1)}(k|\tilde{x}-\tilde{p}|) \\ \qquad \times[-m\sin(m\alpha)(b_i\bar{n}_i)]\Big\}, |\tilde{x}-\tilde{p}|>|\tilde{s}-\tilde{p}|. \end{cases} \tag{41}$$

The kernel function, $M(\tilde{s},\tilde{x})$, can be expanded into

$$M(\tilde{s},\tilde{x})=\sum_{m=0}^{\infty}[\nabla C_m(\tilde{x})\cdot n_x][\nabla R_m(\tilde{s})\cdot n_s]=\begin{cases} M^i=-\dfrac{\pi \mathrm{i}}{2}\displaystyle\sum_{m=0}^{\infty}\varepsilon_m\frac{\partial H_m^{(1)}(k|\tilde{s}-\tilde{p}|)}{\partial n_s}\Big\{\frac{\partial J_m(k|\tilde{x}-\tilde{p}|)}{\partial n_x}\cos(m\alpha) \\ \qquad +J_m(k|\tilde{x}-\tilde{p}|)\dfrac{\partial\cos(m\alpha)}{\partial n_x}\Big\}+\varepsilon_m H_m^{(1)}(k|\tilde{s}-\tilde{p}|)\Big\{\dfrac{\partial J_m(k|\tilde{x}-\tilde{p}|)}{\partial n_x}\dfrac{\partial\cos(m\alpha)}{\partial n_s} \\ \qquad +J_m(k|\tilde{x}-\tilde{p}|)\dfrac{\partial^2\cos(m\alpha)}{\partial n_x\,\partial n_s}\Big\}, |\tilde{s}-\tilde{p}|>|\tilde{x}-\tilde{p}|, \\ M^e=-\dfrac{\pi \mathrm{i}}{2}\displaystyle\sum_{m=0}^{\infty}\varepsilon_m\frac{\partial J_m(k|\tilde{s}-\tilde{p}|)}{\partial n_s}\Big\{\frac{\partial H_m^{(1)}(k|\tilde{x}-\tilde{p}|)}{\partial n_x}\cos(m\alpha)+H_m^{(1)}(k|\tilde{x}-\tilde{p}|) \\ \qquad \times\dfrac{\partial\cos(m\alpha)}{\partial n_x}\Big\}+\varepsilon_m J_m(k|\tilde{s}-\tilde{p}|)\Big\{\dfrac{\partial H_m^{(1)}(k|\tilde{x}-\tilde{p}|)}{\partial n_x}\dfrac{\partial\cos(m\alpha)}{\partial n_s} \\ \qquad +H_m^{(1)}(k|\tilde{x}-\tilde{p}|)\dfrac{\partial^2\cos(m\alpha)}{\partial n_x\,\partial n_s}\Big\}, |\tilde{x}-\tilde{p}|>|\tilde{s}-\tilde{p}|, \end{cases} \tag{42}$$

where

$$\begin{aligned}\frac{\partial^2\cos(m\alpha)}{\partial n_x\partial n_s}&=\frac{\partial[-m\sin(m\alpha)a_in_i]}{\partial n_x}\\ &=a_in_i\frac{\partial[-m\sin(m\alpha)]}{\partial n_x}+(-m\sin(m\alpha))\frac{\partial a_in_i}{\partial n_x}\\ &=a_in_i[-m^2\cos(m\alpha)b_i\bar{n}_i]+[-m\sin(m\alpha)]\\ &\quad\times\Big\{n_1\Big[\frac{-(s_2-p_2)}{|\tilde{s}-\tilde{p}|^3}\Big(\frac{\bar{n}_1}{x_2-p_2}-\frac{(x_1-p_1)\bar{n}_1}{(x_2-p_2)^2}\Big)\Big]\\ &\quad+n_2\Big[\frac{(s_1-p_1)(s_2-p_2)}{|\tilde{s}-\tilde{p}|^3}\Big(\frac{\bar{n}_1}{x_2-p_2}-\frac{(x_1-p_1)\bar{n}_1}{(x_2-p_2)^2}\Big)\Big]\Big\}.\end{aligned} \tag{43}$$

By substituting Eqs. (29)–(31), (36)–(38) and (43) into Eq. (42), we have

$$M(\tilde{s},\tilde{x})\begin{cases} M^i = -\dfrac{\pi \mathrm{i}}{2}\sum\limits_{m=0}^{\infty}\varepsilon_m\Big[\dfrac{k}{2}(H^{(1)}_{m-1}(k|\tilde{s}-\tilde{p}|)-H^{(1)}_{m+1}(k|\tilde{s}-\tilde{p}|))\dfrac{(s_i-p_i)n_i}{|\tilde{s}-\tilde{p}|}\Big]\Big\{\dfrac{k}{2}\Big[J_{m-1}(k|\tilde{x}-\tilde{p}|)-J_{m+1}(k|\tilde{x}-\tilde{p}|)\\ \times\dfrac{(x_i-p_i)\bar{n}_i}{|\tilde{x}-\tilde{p}|}\Big]\cos(m\alpha)+J_m(k|\tilde{x}-\tilde{p}|)[-m\sin(m\alpha)(b_i\bar{n}_i)]\Big\}+\varepsilon_m H^{(1)}_m(k|\tilde{s}-\tilde{p}|)\Big\{\Big[\dfrac{k}{2}(J_{m-1}(k|\tilde{x}-\tilde{p}|)\\ -J_{m+1}(k|\tilde{x}-\tilde{p}|))\dfrac{(x_i-p_i)\bar{n}_i}{|\tilde{x}-\tilde{p}|}\Big][-m\sin(m\alpha)(a_in_i)]+J_m(k|\tilde{x}-\tilde{p}|)[a_in_i(-m^2\cos(m\alpha)b_in_i)+(-m\sin(m\alpha))\\ \times\Big[n_1\Big[\dfrac{-(s_2-p_2)}{|\tilde{s}-\tilde{p}|^3}\Big(\dfrac{\bar{n}_1}{x_2-p_2}-\dfrac{(x_1-p_1)\bar{n}_1}{(x_2-p_2)^2}\Big)\Big]+n_2\Big[\dfrac{(s_1-p_1)(s_2-p_2)}{|\tilde{s}-\tilde{p}|^3}\Big(\dfrac{\bar{n}_1}{x_2-p_2}-\dfrac{(x_1-p_1)\bar{n}_1}{(x_2-p_2)^2}\Big)\Big]\Big]\Big\},\\ |\tilde{s}-\tilde{p}|>|\tilde{x}-\tilde{p}|,\\ M^e = -\dfrac{\pi \mathrm{i}}{2}\sum\limits_{m=0}^{\infty}\varepsilon_m\Big[\dfrac{k}{2}(J_{m-1}(k|\tilde{s}-\tilde{p}|)-J_{m+1}(k|\tilde{s}-\tilde{p}|))\dfrac{(s_i-p_i)n_i}{|\tilde{s}-\tilde{p}|}\Big]\Big\{\dfrac{k}{2}\Big[H^{(1)}_{m-1}(k|\tilde{x}-\tilde{p}|)-H^{(1)}_{m+1}(k|\tilde{x}-\tilde{p}|)\\ \times\dfrac{(x_i-p_i)\bar{n}_i}{|\tilde{x}-\tilde{p}|}\Big]\cos(m\alpha)+H^{(1)}_m(k|\tilde{x}-\tilde{p}|)[-m\sin(m\alpha)(b_i\bar{n}_i)]\Big\}+\varepsilon_m J_m(k|\tilde{s}-\tilde{p}|)\Big\{\Big[\dfrac{k}{2}(H^{(1)}_{m-1}(k|\tilde{x}-\tilde{p}|)\\ -H^{(1)}_{m+1}(k|\tilde{x}-\tilde{p}|))\dfrac{(x_i-p_i)\bar{n}_i}{|\tilde{x}-\tilde{p}|}\Big][-m\sin(m\alpha)(a_in_i)]+H^{(1)}_m(k|\tilde{x}-\tilde{p}|)\Big[a_in_i(-m^2\cos(m\alpha)b_in_i)+(-m\sin(m\alpha))\\ \times\Big[n_1\Big[\dfrac{-(s_2-p_2)}{|\tilde{s}-\tilde{p}|^3}\Big(\dfrac{\bar{n}_1}{x_2-p_2}-\dfrac{(x_1-p_1)\bar{n}_1}{(x_2-p_2)^2}\Big)\Big]+n_2\Big[\dfrac{(s_1-p_1)(s_2-p_2)}{|\tilde{s}-\tilde{p}|^3}\Big(\dfrac{\bar{n}_1}{x_2-p_2}-\dfrac{(x_1-p_1)\bar{n}_1}{(x_2-p_2^2}\Big)\Big]\Big]\Big\},\\ |\tilde{x}-\tilde{p}|>|\tilde{s}-\tilde{p}|. \end{cases} \tag{44}$$

2.4. Dual boundary element formulation in conjunction with the FMM

By employing the constant element scheme after coordinate transformation and moving the center of multipole ($\tilde{p}$) to the center of local coordinate on each boundary element as shown in Fig. 2, each element of the influence matrices can be obtained as follows.

2.4.1. U kernel

For the regular integral ($i \neq j$), we have

(a) $r_{i,j} > 0.5l_j$

$$\begin{aligned} U_{i,j} &= \int_{-0.5l_j}^{0.5l_j} U^e \,\mathrm{d}s = -\frac{\pi \mathrm{i}}{2}\sum_{m=0}^{\infty}\varepsilon_m H^{(1)}_{2m}(kr_{i,j})\cos(2m\alpha)\\ &\quad\times\int_{-0.5l_j}^{0.5l_j} J_m(k|s|)\mathrm{d}s\\ &= -\frac{\pi \mathrm{i}}{2}\sum_{m=0}^{\infty}\varepsilon_m H^{(1)}_{2m}(kr_{i,j})\cos(2m\alpha)\left(\frac{4}{k}\sum_{n=0}^{\infty}J_{2m+2n+1}(0.5l_j)\right)\\ &= \sum_{m=0}^{\infty}C^1_{i,j,m}R_{m,j}, \end{aligned} \tag{45}$$

where $r_{i,j}$ is the distance between the collocation point on ith element's center and the jth source element's center, $r_{i,j} = \sqrt{x_r^2+y_r^2}$, x_r and y_r are the coordinates of collocation point after translation and rotation, l_j is the length of the jth source element. The multipole moment $R_{m,j}$ is the value related to the source point coordinate and $C^1_{i,j,m}$ is the value related to the field point coordinate as shown below:

$$C^1_{i,j,m} = -\frac{\pi \mathrm{i}}{2}\varepsilon_m H^{(1)}_{2m}(kr_{i,j})\cos(2m\alpha), \tag{46}$$

$$R_{m,j} = \frac{4}{k}\sum_{n=0}^{\infty}J_{2m+2n+1}(0.5l_j). \tag{47}$$

(b) $r_{i,j} < 0.5l_j$

$$\begin{aligned} U_{i,j} &= \int_{-0.5l_j}^{-r_{i,j}} U^i \mathrm{d}s + \int_{-r_{i,j}}^{r_{i,j}} U^e \mathrm{d}s + \int_{r_{i,j}}^{0.5l_j} U^i \mathrm{d}s\\ &= -\frac{\pi \mathrm{i}}{2}\sum_{m=0}^{\infty}\varepsilon_m H^{(1)}_{2m}(kr_{i,j})\cos(2m\alpha)\left(\frac{4}{k}\sum_{n=0}^{\infty}J_{2m+2n+1}(kr_{i,j})\right)\\ &\quad -\frac{\pi \mathrm{i}}{2}\sum_{m=0}^{\infty}\varepsilon_m J_{2m}(kr_{i,j})\cos(2m\alpha)2\int_{r_{i,j}}^{0.5l_j}H^{(1)}_{2m}(k|s|)\mathrm{d}s. \end{aligned} \tag{48}$$

For the weakly singular integral ($i = j$), we regularize the integral by means of partial integration and limiting process ($(x_r, y_r) = (0, \epsilon)$) as follows

$$U_{i,i} = \lim_{\epsilon\to 0}\int_{-0.5l_j}^{-\epsilon} U^i\,\mathrm{d}s + \int_{-\epsilon}^{\epsilon} U^e\,\mathrm{d}s + \int_{\epsilon}^{0.5l_j} U^i\,\mathrm{d}s$$
$$= -\frac{\pi\mathrm{i}}{2}\sum_{m=0}^{\infty}\varepsilon_m H_{2m}^{(1)}(k\epsilon)\cos(\pi)\left\{\frac{4}{k}\sum_{n=0}^{n=\infty} J_{2m+2n+1}(k\epsilon) + \frac{-\pi\mathrm{i}}{2}\sum_{m=0}^{\infty}\varepsilon_m J_{2m}(k\epsilon)\cos(\pi)\left(2\int_{\epsilon}^{0.5l_j} H_m^{(1)}(k|s|)\mathrm{d}s\right)\right\}$$
$$= 0 + \frac{-\pi\mathrm{i}}{2}J_0(k\epsilon)\left(2\int_{\epsilon}^{0.5l_j} H_0^{(1)}(k|s|)\mathrm{d}s\right) = \frac{-\pi\mathrm{i}}{2}\left(\int_{-0.5l_j}^{0.5l_j} H_0^{(1)}(k|s|)\mathrm{d}s + \int_{-\epsilon}^{\epsilon} H_0^{(1)}(k|s|)\mathrm{d}s\right)$$
$$= \frac{-\mathrm{i}\pi}{2}\left\{H_0^{(1)}\left(\frac{kl}{2}\right)l\right\} + k\int_{-0.5l_j}^{0.5l_j} H_1^{(1)}(k|s|)|s|\mathrm{d}s), \tag{49}$$

where

$$\lim_{\epsilon\to 0}\int_{-\epsilon}^{\epsilon} H_0^{(1)}(k|s|)\mathrm{d}s = \lim_{\epsilon\to 0}\int_{-\epsilon}^{\epsilon}\frac{2i}{\pi}\ln(ks)\mathrm{d}s = 0. \tag{50}$$

2.4.2. T kernel

For the regular integral ($i \neq j$), we have

(a) $r_{i,j} > 0.5l$

$$T_{i,j} = \int_{-0.5l_j}^{0.5l_j} T^e\,\mathrm{d}s = -\frac{\pi\mathrm{i}}{2}\sum_{m=0}^{\infty}\varepsilon_m H_{2m}^{(1)}(kr_{i,j})\cos(2m\alpha)\int_{-0.5l_j}^{0.5l_j}\frac{k}{2}[J_{2m-1}(k|s|) - J_{2m+1}(k|s|)]\frac{s\cdot 0 + 0\cdot(-1)}{|s|}\mathrm{d}s$$
$$-\frac{\pi\mathrm{i}}{2}\sum_{m=0}^{\infty} 2H_{2m+1}^{(1)}(kr_{i,j})(2m+1)\sin((2m+1)\alpha)\int_{-0.5l_j}^{0.5l_j}\frac{-J_{2m+1}(k|s|)}{|s|}\mathrm{d}s \tag{51}$$
$$= \pi\mathrm{i}\sum_{m=0}^{\infty} H_{2m+1}^{(1)}(kr_{i,j})(2m+1)\sin((2m+1)\alpha)\frac{k}{4m+2}\int_{-0.5l_j}^{0.5l_j}[J_{2m}(k|s|) + J_{2m+2}(k|s|)]\mathrm{d}s = C_{i,j,m}^2[R_{m,j} + R_{(m+1),j}],$$

where

$$C_{i,j,m}^2 = \pi\mathrm{i}H_{2m+1}^{(1)}(kr_{i,j})(2m+1)\sin((2m+1)\alpha)\frac{k}{4m+2}. \tag{52}$$

(b) $r_{i,j} < 0.5l$

$$T_{i,j} = \int_{-0.5l_j}^{-r_{i,j}} T^i\,\mathrm{d}s + \int_{-r_{i,s}}^{r_{i,s}} T^e\,\mathrm{d}s + \int_{r_{i,j}}^{0.5l_j} T^i\,\mathrm{d}s = \pi\mathrm{i}\sum_{m=0}^{\infty} H_{2m+1}^{(1)}(kr_{i,j})(2m+1)\sin((2m+1)\alpha)\int_{-r_{i,j}}^{r_{i,j}}\frac{J_{2m+1}(k|s|)}{|s|}\mathrm{d}s$$
$$+\pi\mathrm{i}\sum_{m=0}^{\infty} J_{2m+1}(kr_{i,j})(2m+1)\sin((2m+1)\alpha)(2)\int_{r_{i,j}}^{0.5l_j}\frac{H_{2m+1}^{(1)}(k|s|)}{|s|}\mathrm{d}s = \pi\mathrm{i}\sum_{m=0}^{\infty} H_{2m+1}^{(1)}(kr_{i,j})(2m+1)\sin((2m+1)\alpha)$$
$$\times\frac{k}{4m+2}\int_{-r_{i,j}}^{r_{i,j}}[J_{2m}(k|s|) + J_{2m+2}(k|s|)]\mathrm{d}s + \pi\mathrm{i}\sum_{m=0}^{\infty} J_{2m+1}(kr_{i,j})(2m+1)\sin((2m+1)\alpha)(2)\frac{k}{4m+2}\int_{r_{i,j}}^{0.5l_j}[H_{2m}^{(1)}(k|s|)$$
$$+ H_{2m+2}^{(1)}(k|s|)]\mathrm{d}s. \tag{53}$$

For the strongly singular integral ($i=j$), we regularize the integral by means of partial integration, limiting process and the identities from the generalized function as shown below [19]

$$\sum_{m=1}^{\infty}\frac{\sin\left(m\frac{\pi}{2}\right)}{m} = \frac{\pi}{4}. \tag{54}$$

We can obtain the integral as follows

$$T_{i,i}=\int_{-0.5l_j}^{-\epsilon} T^i\,\mathrm{d}s+\int_{-\epsilon}^{-\epsilon} T^e\,\mathrm{d}s+\int_{\epsilon}^{0.5l_j} T^i\,\mathrm{d}s=\pi\mathrm{i}\sum_{m=0}^{\infty} H_{2m+1}^{(1)}(kr_{i,j})(2m+1)\sin\left((2m+1)\frac{\pi}{2}\right)\int_{-\epsilon}^{\epsilon}\frac{J_{2m+1}(k|s|)}{|s|}\mathrm{d}s$$
$$+2\pi\mathrm{i}\sum_{m=0}^{\infty} J_{2m+1}(k\epsilon)(2m+1)\sin\left((2m+1)\frac{\pi}{2}\right)\int_{\epsilon}^{0.5l_j}\frac{H_{2m+1}^{(1)}(k|s|)}{|s|}\mathrm{d}s=2\sum_{m=0}^{\infty}\frac{(-1)^m}{\epsilon^{2m+1}}\int_0^{\epsilon}s^{2m}\,\mathrm{d}s+2\sum_{m=0}^{\infty}(-1)^m\epsilon^{2m+1}$$
$$\times\int_{\epsilon}^{\sqrt{\epsilon}}\frac{1}{s^{2m}}\mathrm{d}s=2\sum_{m=0}^{\infty}\frac{(-1)^m}{2m+1}+2\sum_{m=0}^{\infty}\frac{(-1)^m}{2m+1}=2\sum_{m=1}^{\infty}\frac{\sin\left(m\frac{\pi}{2}\right)}{m}+2\sum_{m=1}^{\infty}\frac{\sin\left(m\frac{\pi}{2}\right)}{m}=\pi, \tag{55}$$

where

$$\lim_{\epsilon\to 0}J_{2m+1}(k\epsilon)\int_{\sqrt{\epsilon}}^{0.5l_j}\frac{H_{2m+1}^{(1)}(k|s|)}{|s|}\mathrm{d}s$$
$$=\int_{\sqrt{\epsilon}}^{0.5l_j}\lim_{\epsilon\to 0}\frac{(2m+1)(k\epsilon)^{2m+1}}{2^{2m+1}(2m+1)!}\frac{H_{2m+1}^{(1)}(k|s|)}{|s|}\mathrm{d}s=0. \tag{56}$$

2.4.3. L kernel

For the regular integral ($i\neq j$), we have

(a) $r_{i,j}>0.5l$

$$L_{i,j}=\int_{-0.5l_j}^{0.5l_j}L^e\,\mathrm{d}s=-\frac{\pi\mathrm{i}}{2}\sum_{m=0}^{\infty}\varepsilon_m\frac{k}{2}[H_{2m-1}^{(1)}(kr_{i,j})$$
$$-H_{2m+1}^{(1)}(kr_{i,j})]\frac{x_i\bar{n}_i}{r_{i,j}}\cos(2m\alpha)\int_{-0.5l_j}^{0.5l_j}J_{2m}(k|s|)\mathrm{d}s$$
$$-\frac{\pi\mathrm{i}}{2}\sum_{m=0}^{\infty}\varepsilon_m H_{2m}^{(1)}(kr_{i,j})(2m)\sin(2m\alpha)\frac{y_r\bar{n}_1-x_r\bar{n}_2}{r_{i,j}^2}$$
$$\times\int_{-0.5l_j}^{0.5l_j}J_{2m}(k|s|)\mathrm{d}s=\sum_{m=0}^{\infty}C_{i,j,m}^3R_{m,j}, \tag{57}$$

where

$$C_{i,j,m}^3=-\frac{\pi\mathrm{i}}{2}\varepsilon_m\left\{\frac{k}{2}[H_{2m-1}^{(1)}(kr_{i,j})-H_{2m+1}^{(1)}(kr_{i,j})]\frac{x_i\bar{n}_i}{r_{i,j}}\right.$$
$$\left.\times\cos(2m\alpha)+H_{2m}^{(1)}(kr_{i,j})(2m)\sin(2m\alpha)\frac{y_r\bar{n}_1-x_r\bar{n}_2}{r_{i,j}^2}\right\}. \tag{58}$$

(b) $r_{i,j}<0.5l$

$$L_{i,j}=\int_{-0.5l_j}^{-r_{i,j}}L^i\mathrm{d}s+\int_{-r_{i,j}}^{r_{i,j}}L^e\mathrm{d}s+\int_{r_{i,j}}^{0.5l_j}L^i\mathrm{d}s$$
$$=-\frac{\pi\mathrm{i}}{2}\sum_{m=0}^{\infty}\varepsilon_m\frac{k}{2}[H_{2m-1}^{(1)}(kr_{i,j})-H_{2m+1}^{(1)}(kr_{i,j})]\frac{x_i\bar{n}_i}{r_{i,j}}\cos(2m\alpha)$$
$$\times\int_{-0.5l_j}^{0.5l_j}J_{2m}(k|s|)\mathrm{d}s-\frac{\pi\mathrm{i}}{2}\sum_{m=0}^{\infty}\varepsilon_m H_{2m}^{(1)}(kr_{i,j})(2m)\sin(2m\alpha)$$
$$\times\frac{y_r\bar{n}_1-x_r\bar{n}_2}{r_{i,j}^2}\int_{-0.5l_j}^{0.5l_j}J_{2m}(k|s|)\mathrm{d}s-\frac{\pi\mathrm{i}}{2}\sum_{m=0}^{\infty}\varepsilon_m\frac{k}{2}[J_{2m-1}(kr_{i,j})$$
$$-J_{2m+1}(kr_{i,j})]\frac{x_i\bar{n}_i}{r_{i,j}}\cos(2m\alpha)\left(2\int_{r_{i,j}}^{0.5l_j}H_{2m}^{(1)}(k|s|\mathrm{d}s)\right)$$
$$-\frac{\pi\mathrm{i}}{2}\sum_{m=0}^{\infty}\varepsilon_m J_{2m}(kr_{i,j})(2m)\sin(2m\alpha)\frac{y_r\bar{n}_1-x_r\bar{n}_2}{r_{i,j}^2}$$
$$\times\left(2\int_{r_{i,j}}^{0.5l_j}H_{2m}^{(1)}(k|s|)\mathrm{d}s\right). \tag{59}$$

For the strongly singular integral ($i=j$), we regularize the integral by means of partial integration and limiting process as follows

$$L_{i,i}=\int_{-0.5l_j}^{-\epsilon}L^i\mathrm{d}s+\int_{-\epsilon}^{\epsilon}L^e\mathrm{d}s+\int_{\epsilon}^{0.5l_j}L^i\mathrm{d}s$$
$$=\frac{-\pi\mathrm{i}}{2}\sum_{m=0}^{\infty}\varepsilon_m\frac{k}{2}[H_{2m-1}^{(1)}(k|\epsilon|)-H_{2m+1}^{(1)}(k|\epsilon|)](-1)^m$$
$$\times\int_{-\epsilon}^{\epsilon}J_{2m}(k|s|)\mathrm{d}s+\frac{-\pi\mathrm{i}}{2}\sum_{m=0}^{\infty}\varepsilon_m\frac{k}{2}[J_{2m-1}(k|\epsilon|)$$
$$-J_{2m+1}(k|\epsilon|)](-1)^m\left(2\int_{\epsilon}^{0.5l_j}H_{2m}^{(1)}(k|s|)\mathrm{d}s\right)$$
$$=-2\sum_{m=1}^{\infty}\frac{(-1)^m}{\epsilon^{2m+1}}\int_0^{\epsilon}s^{2m}\mathrm{d}s-2+\sum_{m=1}^{\infty}(-1)^m\epsilon^{2m-1}\int_{\epsilon}^{\sqrt{\epsilon}}\frac{2}{s^{2m}}\mathrm{d}s$$
$$=-2\sum_{m=1}^{\infty}\frac{(-1)^m}{2m+1}-2-2\sum_{m=1}^{\infty}\frac{(-1)^m}{1-2m}$$
$$=-2\left[\sum_{m=1}^{\infty}\frac{\sin(m\frac{\pi}{2})}{m}-1\right]-2-2\left[\sum_{m=1}^{\infty}\frac{\sin(m\frac{\pi}{2})}{m}\right]=-\pi, \tag{60}$$

where

$$\lim_{\epsilon\to 0}[J_{2m-1}(k|\epsilon|)-J_{2m+1}(k|\epsilon|)]\int_{\sqrt{\epsilon}}^{0.5l_j}H_{2m}^{(1)}(k|s|)\mathrm{d}s=0. \tag{61}$$

2.4.4. M kernel

For the regular integral ($i\neq j$), we have

(a) $r_{i,j}>0.5l$

$$M_{i,j}=\int_{-0.5l_j}^{0.5l_j}M^e\,\mathrm{d}s=\frac{\pi\mathrm{i}}{2}\sum_{m=0}^{\infty}(2)\frac{k}{2}[H_{2m}^{(1)}(kr_{i,j})$$
$$-H_{2m+2}^{(1)}(kr_{i,j})]\frac{x_i\bar{n}_i}{r_{i,j}}[(2m+1)\sin((2m+1)\alpha)]$$
$$\times\int_{-0.5l_j}^{0.5l_j}\frac{J_{2m}(k|s|)}{|s|}\mathrm{d}s+\frac{\pi\mathrm{i}}{2}\sum_{m=0}^{\infty}(2)H_{2m+1}^{(1)}(kr_{i,j})$$
$$\times(2m+1)\cos((2m+1)\alpha)\frac{y_r\bar{n}_1-x_r\bar{n}_2}{r_{i,j}^2}$$
$$\times\int_{-0.5l_j}^{0.5l_j}\frac{J_{2m}(k|s|)}{|s|}\mathrm{d}s=\sum_{m=0}^{\infty}C_{i,j,m}^4[R_{m,j}+R_{(m+1),j}], \tag{62}$$

where

$$C^4_{i,j,m} = \frac{\pi \mathrm{i}}{r^2_{i,j}}(2m+1)\frac{k}{2}\Bigg\{(r_{i,j})[H^{(1)}_{2m}(kr_{i,j}) - H^{(1)}_{2m+2}(kr_{i,j})]\frac{x_i\bar{n}_i}{r_{i,j}}\sin((2m+1)\alpha) + H^{(1)}_{2m+1}(kr_{i,j})(2m+1)\cos((2m+1)\alpha) \times \frac{y_r\bar{n}_1 - x_r\bar{n}_2}{r^2_{i,j}}\Bigg\}. \tag{63}$$

(b) $r_{i,j} < 0.5l$

$$M_{i,j} = \int_{-0.5l_j}^{-r_{i,j}} M^i \,\mathrm{d}s + \int_{-r_{i,j}}^{r_{i,j}} M^e \,\mathrm{d}s + \int_{r_{i,j}}^{0.5l_j} M^i \,\mathrm{d}s = \frac{\pi \mathrm{i}}{r^2_{i,j}}\sum_{m=0}^{\infty}(2m+1)\Bigg\{\frac{k}{2}(r_{i,j})[H^{(1)}_{2m}(kr_{i,j}) - H^{(1)}_{2m+2}(kr_{i,j})]x_i\bar{n}_i\sin((2m+1)\alpha) + H^{(1)}_{2m+1}(kr_{i,j})(2m+1)\cos((2m+1)\alpha)y_r\bar{n}_1 - x_r\bar{n}_2\Bigg\}\frac{k}{4m+2}\int_{-r_{i,j}}^{r_{i,j}}[J_{2m}(k|s|) + J_{2m+2}(k|s|)]\mathrm{d}s + \frac{\pi \mathrm{i}}{r^2_{i,j}}\sum_{m=0}^{\infty}(2m+1) \times\Bigg\{\frac{k}{2}(r_{i,j})[J_{2m}(kr_{i,j}) - J_{2m+2}(kr_{i,j})]x_i\bar{n}_i\sin((2m+1)\alpha) + J_{2m+1}(kr_{i,j})(2m+1)\cos((2m+1)\alpha)y_r\bar{n}_1 - x_r\bar{n}_2\Bigg\} \times \frac{k}{4m+2}\int_{r_{i,j}}^{0.5l_j}[H^{(1)}_{2m}(k|s|) + H^{(1)}_{2m+2}(k|s|)]\mathrm{d}s. \tag{64}$$

For the hypersingular integral ($i = j$), we regularize the integral by means of partial integration, limiting process and using the identities from the generalized function as shown below [19]

$$\sum_{m=0}^{\infty}(-1)^m = \frac{1}{2}. \tag{65}$$

We can obtain the integral as follows:

$$M_{i,i} = \int_{-0.5l_j}^{-\epsilon} M^i \,\mathrm{d}s + \int_{-\epsilon}^{\epsilon} M^e \,\mathrm{d}s + \int_{\epsilon}^{0.5l_j} M^i \,\mathrm{d}s = -\mathrm{i}\pi k\Bigg\{\int_{\epsilon}^{0.5l_j}\frac{H^{(1)}_1(k|s|)}{|s|}\mathrm{d}s + \sum_{m=1}^{\infty}J_{2m}(k\epsilon)(2m+1)(-1)^m \times\int_{\epsilon}^{0.5l_j}\frac{H^{(1)}_{2m+1}(k|s|)}{|s|}\mathrm{d}s\Bigg\} + \sum_{m=1}^{\infty}\frac{2(2m+1)(-1)^m}{\epsilon^{2m+2}}\int_0^{\epsilon}s^{2m}\,\mathrm{d}s = \frac{-\mathrm{i}\pi k}{2}\Bigg\{-2H^{(1)}_1\Big(\frac{kl}{2}\Big) + k\Bigg[H^{(1)}_0\Big(\frac{kl}{2}\Big) + k\int_{-0.5l}^{0.5l_j}H^{(1)}_1(k|s|)|s|\mathrm{d}s\Bigg]\Bigg\} - \frac{2}{\epsilon} + \frac{2}{\epsilon}\sum_{m=1}^{\infty}(-1)^{m-1} + \frac{2}{\epsilon}\sum_{m=0}^{\infty}(-1)^m = \frac{-\mathrm{i}\pi k}{2}\Bigg\{-2H^{(1)}_1\Big(\frac{kl}{2}\Big) + k\Bigg[H^{(1)}_0\Big(\frac{kl}{2}\Big) + k\int_{-0.5l}^{0.5l_j}H^{(1)}_1(k|s|)|s|\mathrm{d}s\Bigg]\Bigg\} = i\pi kH^{(1)}_1\Big(\frac{kl}{2}\Big) - \frac{i\pi k^2}{2}U_{i,i}. \tag{66}$$

$$\Bigg\{\sum_{m=0}^{\infty}\begin{bmatrix} 0 & C^2_{1,2,m}(R_{m,2}+R_{(m+1),2}) & \cdots & C^2_{1,N,m}(R_{m,N}+R_{(m+1),N}) \\ C^2_{2,1,m}(R_{m,1}+R_{(m+1),1}) & 0 & \cdots & C^2_{2,N,m}(R_{m,N}+R_{(m+1),N}) \\ \vdots & \vdots & \ddots & \vdots \\ C^2_{N,1,m}(R_{m,1}+R_{(m+1),1}) & C^2_{N,2,m}(R_{m,2}+R_{(m+1),2}) & \cdots & 0 \end{bmatrix} + \pi\mathrm{i}\Bigg\}\begin{Bmatrix} u_1 \\ u_2 \\ \vdots \\ u_N \end{Bmatrix}$$

$$= \Bigg\{\sum_{m=0}^{\infty}\begin{bmatrix} 0 & C^1_{1,2,m}R_{m,2} & \cdots & C^1_{1,N,m}R_{m,N} \\ C^1_{2,1,m}R_{m,1} & 0 & \cdots & C^1_{2,N,m}R_{m,N} \\ \vdots & \vdots & \ddots & \vdots \\ C^1_{N,1,m}R_{m,1} & C^1_{N,2,m}R_{m,2} & \cdots & 0 \end{bmatrix} + [\mathrm{diag}(U_{i,i})]\Bigg\}\begin{Bmatrix} t_1 \\ t_2 \\ \vdots \\ t_N \end{Bmatrix}. \tag{67}$$

It is interesting to find that $R_{m,j}$ term is embedded in the formula of the four influence matrices of Eqs. (45), (51), (57) and (62).

2.5. Construction of the four influence matrices

By using Eqs. (45) and (51), the algebraic system *UT* equation of the dual boundary integral formulation in Eq. (18) can be rewritten as

By using Eqs. (57) and (62), the algebraic system of the *LM* equation of the dual boundary integral formulation of Eq. (19) can be rewritten as

$$\left\{\sum_{m=0}^{\infty}\begin{bmatrix} 0 & C^4_{1,2,m}(R_{m,2}+R_{(m+1),2}) & \cdots & C^4_{1,N,m}(R_{m,N}+R_{(m+1),N}) \\ C^4_{2,1,m}(R_{m,1}+R_{(m+1),1}) & 0 & \cdots & C^4_{2,N,m}(R_{m,N}+R_{(m+1),N}) \\ \vdots & \vdots & \ddots & \vdots \\ C^4_{N,1,m}(R_{m,1}+R_{(m+1),1}) & C^4_{N,2,m}(R_{m,2}+R_{(m+1),2}) & \cdots & 0 \end{bmatrix} + [\mathrm{diag}(M_{i,i})]\right\}\begin{Bmatrix} u_1 \\ u_2 \\ \vdots \\ u_N \end{Bmatrix}$$

$$= \left\{\sum_{m=0}^{\infty}\begin{bmatrix} 0 & C^3_{1,2,m}R_{m,2} & \cdots & C^3_{1,N,m}R_{m,N} \\ C^3_{2,1,m}R_{m,1} & 0 & \cdots & C^3_{2,N,m}R_{m,N} \\ \vdots & \vdots & \ddots & \vdots \\ C^3_{N,1,m}R_{m,1} & C^3_{N,2,m}R_{m,2} & \cdots & 0 \end{bmatrix} + \pi[I]\right\}\begin{Bmatrix} t_1 \\ t_2 \\ \vdots \\ t_N \end{Bmatrix}. \tag{68}$$

where I is the unit matrix.

By adopting the $M+1$ terms in the series sum, the four influence matrices can be rewritten as

$$[U] = \begin{bmatrix} 0 & 0 & \cdots & 0 \\ C^1_{2,1,0} & C^1_{2,1,1} & \cdots & C^1_{2,1,M} \\ \vdots & \vdots & \ddots & \vdots \\ C^1_{N,1,0} & C^1_{N,1,1} & \cdots & C^1_{N,1,M} \end{bmatrix}_{N\times(M+1)}\begin{bmatrix} R_{0,1} & 0 & \cdots & 0 \\ R_{1,1} & 0 & \cdots & 0 \\ \vdots & \vdots & \ddots & \vdots \\ R_{M,1} & 0 & \cdots & 0 \end{bmatrix}_{(M+1)\times N} + \begin{bmatrix} C^1_{1,2,0} & C^1_{1,2,1} & \cdots & C^1_{1,2,M} \\ 0 & 0 & \cdots & 0 \\ \vdots & \vdots & \ddots & \vdots \\ C^1_{N,2,0} & C^1_{N,2,1} & \cdots & C^1_{N,2,M} \end{bmatrix}_{N\times(M+1)}$$
$$\times\begin{bmatrix} 0 & R_{0,2} & \cdots & 0 \\ 0 & R_{1,2} & \cdots & 0 \\ \vdots & \vdots & \ddots & \vdots \\ 0 & R_{M,2} & \cdots & 0 \end{bmatrix}_{(M+1)\times N} + \cdots + \begin{bmatrix} C^1_{1,N,0} & C^1_{1,N,1} & \cdots & C^1_{1,N,M} \\ C^1_{2,N,0} & C^1_{2,N,1} & \cdots & C^1_{2,N,M} \\ \vdots & \vdots & \ddots & \vdots \\ 0 & 0 & \cdots & 0 \end{bmatrix}_{N\times(M+1)}\begin{bmatrix} 0 & 0 & \cdots & R_{0,N} \\ 0 & 0 & \cdots & R_{1,N} \\ \vdots & \vdots & \ddots & \vdots \\ 0 & 0 & \cdots & R_{M,N} \end{bmatrix}_{(M+1)\times N}$$
$$+ [\mathrm{diag}(U_{i,i})]_{N\times N}, \tag{69}$$

$$[T] = \begin{bmatrix} 0 & 0 & \cdots & 0 \\ C^2_{2,1,0} & C^2_{2,1,1} & \cdots & C^2_{2,1,M} \\ \vdots & \vdots & \ddots & \vdots \\ C^2_{N,1,0} & C^2_{N,1,1} & \cdots & C^2_{N,1,M} \end{bmatrix}_{N\times(M+1)}\begin{bmatrix} (R_{0,1}+R_{1,1}) & 0 & \cdots & 0 \\ (R_{1,1}+R_{2,1}) & 0 & \cdots & 0 \\ \vdots & \vdots & \ddots & \vdots \\ (R_{M,1}+R_{(M+1),1}) & 0 & \cdots & 0 \end{bmatrix}_{(M+1)\times N} + \begin{bmatrix} C^2_{1,2,0} & C^2_{1,2,1} & \cdots & C^2_{1,2,M} \\ 0 & 0 & \cdots & 0 \\ \vdots & \vdots & \ddots & \vdots \\ C^2_{N,2,0} & C^2_{N,2,1} & \cdots & C^2_{N,2,M} \end{bmatrix}_{N\times(M+1)}$$
$$\times\begin{bmatrix} 0 & (R_{0,2}+R_{1,2}) & \cdots & 0 \\ 0 & (R_{1,2}+R_{2,2}) & \cdots & 0 \\ \vdots & \vdots & \ddots & \vdots \\ 0 & (R_{M,2}+R_{(M+1),2}) & \vdots & 0 \end{bmatrix}_{(M+1)\times N} + \cdots + \begin{bmatrix} C^2_{1,N,0} & C^2_{1,N,1} & \cdots & C^2_{1,N,M} \\ C^2_{2,N,0} & C^2_{2,N,1} & \cdots & C^2_{2,N,M} \\ \vdots & \vdots & \ddots & \vdots \\ 0 & 0 & \cdots & 0 \end{bmatrix}_{N\times(M+1)}\begin{bmatrix} 0 & 0 & \cdots & (R_{0,N}+R_{1,N}) \\ 0 & 0 & \cdots & (R_{1,N}+R_{2,N}) \\ \vdots & \vdots & \ddots & \vdots \\ 0 & 0 & \cdots & (R_{M,N}+R_{(M+1),N}) \end{bmatrix}_{(M+1)\times N} + \pi[\mathrm{I}], \tag{70}$$

$$
[L] = \begin{bmatrix} 0 & 0 & \cdots & 0 \\ C^3_{2,1,0} & C^3_{2,1,1} & \cdots & C^3_{2,1,M} \\ \vdots & \vdots & \ddots & \vdots \\ C^3_{N,1,0} & C^3_{N,1,1} & \cdots & C^3_{N,1,M} \end{bmatrix}_{N\times(M+1)} \begin{bmatrix} R_{0,1} & 0 & \cdots & 0 \\ R_{1,1} & 0 & \cdots & 0 \\ \vdots & \vdots & \ddots & \vdots \\ R_{M,1} & 0 & \cdots & 0 \end{bmatrix}_{(M+1)\times N} .
$$

$$
+ \begin{bmatrix} C^3_{1,2,0} & C^3_{1,2,1} & \cdots & C^3_{1,2,M} \\ 0 & 0 & \cdots & 0 \\ \vdots & \vdots & \ddots & \vdots \\ C^3_{N,2,0} & C^3_{N,2,1} & \cdots & C^3_{N,2,M} \end{bmatrix}_{N\times(M+1)} \begin{bmatrix} 0 & R_{0,2} & \cdots & 0 \\ 0 & R_{1,2} & \cdots & 0 \\ \vdots & \vdots & \ddots & \vdots \\ 0 & R_{M,2} & \cdots & 0 \end{bmatrix}_{(M+1)\times N} .
$$

$$
+ \cdots + \begin{bmatrix} C^3_{1,N,0} & C^3_{1,N,1} & \cdots & C^3_{1,N,M} \\ C^3_{2,N,0} & C^3_{2,N,1} & \cdots & C^3_{2,N,M} \\ \vdots & \vdots & \ddots & \vdots \\ 0 & 0 & \cdots & 0 \end{bmatrix}_{N\times(M+1)} \begin{bmatrix} 0 & 0 & \cdots & R_{0,N} \\ 0 & 0 & \cdots & R_{1,N} \\ \vdots & \vdots & \ddots & \vdots \\ 0 & 0 & \cdots & R_{M,N} \end{bmatrix}_{(M+1)\times N} + \pi[I], \tag{71}
$$

$$
[M] = \begin{bmatrix} 0 & 0 & \cdots & 0 \\ C^4_{2,1,0} & C^4_{2,1,1} & \cdots & C^4_{2,1,M} \\ \vdots & \vdots & \ddots & \vdots \\ C^4_{N,1,0} & C^4_{N,1,1} & \cdots & C^4_{N,1,M} \end{bmatrix}_{N\times(M+1)} \begin{bmatrix} (R_{0,1}+R_{1,1}) & 0 & \cdots & 0 \\ (R_{1,1}+R_{2,1}) & 0 & \cdots & 0 \\ \vdots & \vdots & \ddots & \vdots \\ (R_{M,1}+R_{(M+1),1}) & 0 & \cdots & 0 \end{bmatrix}_{(M+1)\times N} .
$$

$$
+ \begin{bmatrix} C^4_{1,2,0} & C^4_{1,2,1} & \cdots & C^4_{1,2,M} \\ 0 & 0 & \cdots & 0 \\ \vdots & \vdots & \ddots & \vdots \\ C^4_{N,2,0} & C^4_{N,2,1} & \cdots & C^4_{N,2,M} \end{bmatrix}_{N\times(M+1)} \begin{bmatrix} 0 & (R_{0,2}+R_{1,2}) & \cdots & 0 \\ 0 & (R_{1,2}+R_{2,2}) & \cdots & 0 \\ \vdots & \vdots & \ddots & \vdots \\ 0 & (R_{M,2}+R_{(M+1),2}) & \cdots & 0 \end{bmatrix}_{(M+1)\times N}
$$

$$
+ \cdots + \begin{bmatrix} C^4_{1,N,0} & C^4_{1,N,1} & \cdots & C^4_{1,N,M} \\ C^2_{2,N,0} & C^2_{2,N,1} & \cdots & C^2_{2,N,M} \\ \vdots & \vdots & \ddots & \vdots \\ 0 & 0 & \cdots & 0 \end{bmatrix}_{N\times(M+1)} \begin{bmatrix} 0 & 0 & \cdots & (R_{0,N}+R_{1,N}) \\ 0 & 0 & \cdots & (R_{1,N}+R_{2,N}) \\ \vdots & \vdots & \ddots & \vdots \\ 0 & 0 & \cdots & (R_{M,N}+R_{(M+1),N}) \end{bmatrix}_{(M+1)\times N} + [\mathrm{diag}(M_{i,i})]_{N\times N}. \tag{72}
$$

It is interesting that the four influence matrices in the dual BEM are all composed of the field point matrices and the source point matrices. The separable technique can promote the efficiency in determing the influence coefficients. The source point matrices of $[U]$ are all the same with $[L]$, while the source point matrices of $[T]$ are all the same with $[M]$. Besides, many influence coefficients in the source point matrices of $[T]$ and $[M]$ have the same value with $[U]$ and $[L]$, or with only some combinations. There are many zeros or the same influence coefficients in the field point matrices decomposed in the four influence matrices. Therefore, we can avoid calculating repeatedly the same term. The separable technique reduces the number of floating-point operations from $O(N^2)$ to $O(N\log^a(N))$. Thus, large computation time savings are achieved and memory requirements are reduced, thus enabling us apply BEM to solve large-scale problems.

3. Illustrative examples

To demonstrate the validity of the dual integral formulation in conjunction with the FMM, two examples for scattering problem by an infinite cylinder with radius (a) subject to the Neumann boundary condition are given as follows.

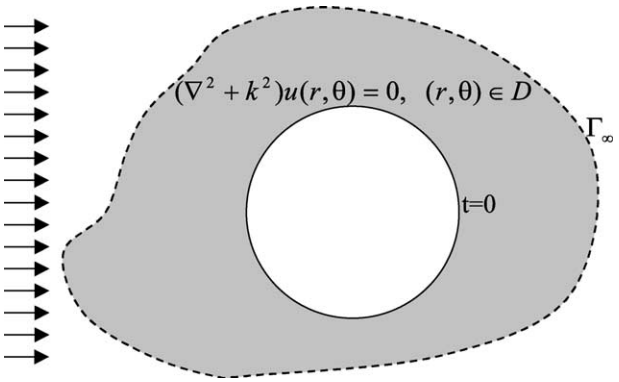

Fig. 4. The scattering problem for a cylinder with the Neumann boundary condition.

Example 1. The radius, a, is 5 m and the wave number of incident wave, k, is 4π.

In the Example 1, we solve the problem by applying the *LU* decomposition in the developed program and compare with the analytical solution and the conventional dual BEM. The problem was chosen because the analytical solution is known [23,35]. It is therefore a good model problem to test the accuracy of DBEM by employing the concept of FMM. The example is shown in Fig. 4 and the analytical solution is

$$u(r,\theta) = -\frac{J_0'(ka)}{H_0^{(1)'}(ka)} H_0^{(1)}(kr) - 2\sum_{n=1}^{\infty} \mathrm{i}^n \frac{J_n'(ka)}{H_n^{(1)'}(ka)} \times H_n^{(1)}(kr)\cos(n\theta), \tag{73}$$

where $\mathrm{i}^2 = -1$. Fig. 5 shows the contour plots of the real-part solutions for the case of $ka = 20\pi$. The unknown boundary solutions of scattering field using the boundary mesh of 100 elements, Re(u) and Im(u), are plotted in Figs. 6 and 7 and 800 elements in Figs. 8 and 9. Solution using the uniform mesh refinement of 800 elements converges to the exact solution. By adopting only four moment FMM formulation, the results are compared well with those of FEM, conventional BEM and analytical solutions. Comparison of error norms for the FMM results versus different terms in the series is shown in Fig. 10. Fig. 11 shows the error norms against different meshes. Only a few terms in the FMM can reach within the error tolerance. Comparison of CPU time using the FMM with different terms are plotted in Fig. 12. Fig. 13 shows the CPU time versus different meshes. The trend of CPU time in proportional to N^2 and $N \log^{2.5} N$ is found for the conventional BEM and the FMM, respectively.

Example 2. The radius, a, is 50 m and the wave number of incident wave, k, is π. Fig. 14 shows the contour plots of the real-part solutions for the case of $ka = 50\pi$. The unknown boundary solution of scattering field using the mesh of 400 elements, Re(u) and Im(u), are plotted in Figs. 15 and 16 and in Figs. 17 and 18 using 1100 elements. Solution using the uniform mesh refinement of 1100 elements converges to the exact solution. By adopting

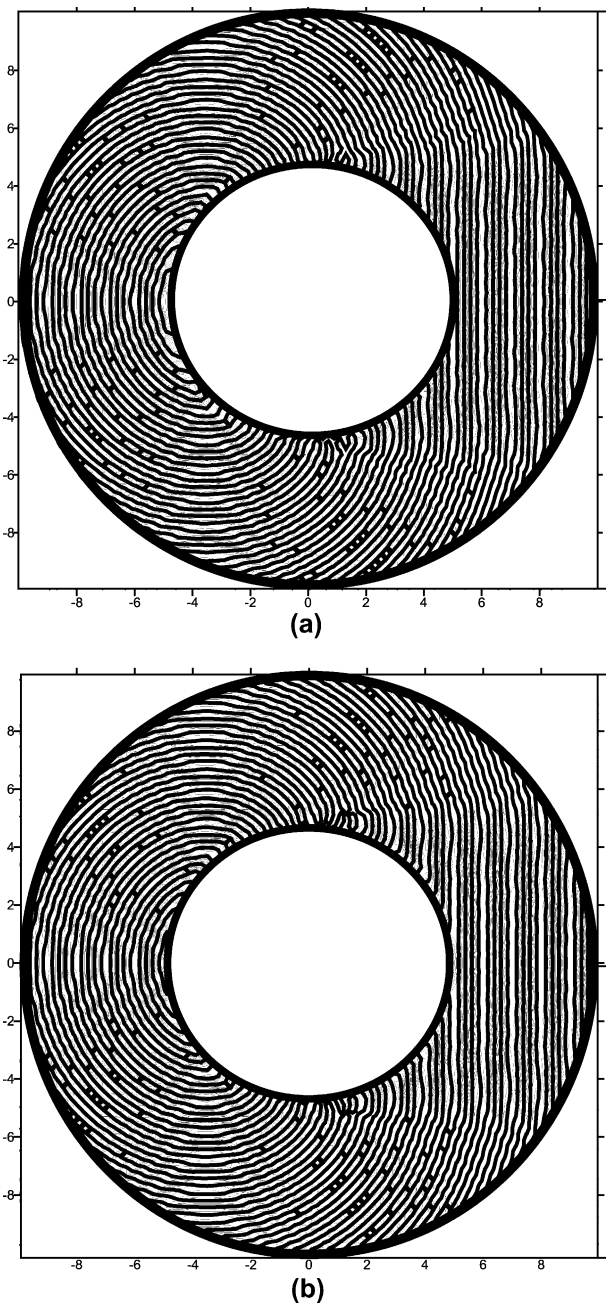

Fig. 5. The contour plot of the real-part solutions in the case 1. (a) Exact solution, (b) FMM results ($M = 4$).

only three moment FMM formulation, the results are compared well with those of FEM, conventional BEM and analytical solutions. Comparison of error norms for the FMM results versus different terms in the series is shown in Fig. 19. Fig. 20 shows the error norms against different meshes. Only a few terms in the FMM can reach within the error tolerance. Comparison of CPU time using the FMM with different terms are plotted in Fig. 21. Fig. 22 shows the CPU time versus different meshes. The FMM can reduce CPU time thus enabling us apply BEM to solve for

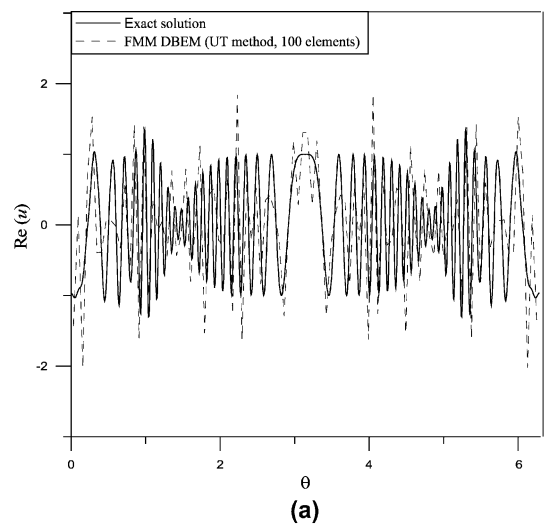

Fig. 6. The boundary solution of the scattering field using 100 boundary elements, Re(u), for the case 1. (a) *UT* equation of FMM ($M = 4$), (b) *LM* equation of FMM ($M = 4$), (c) Burton and Miller method of FMM ($M = 4$).

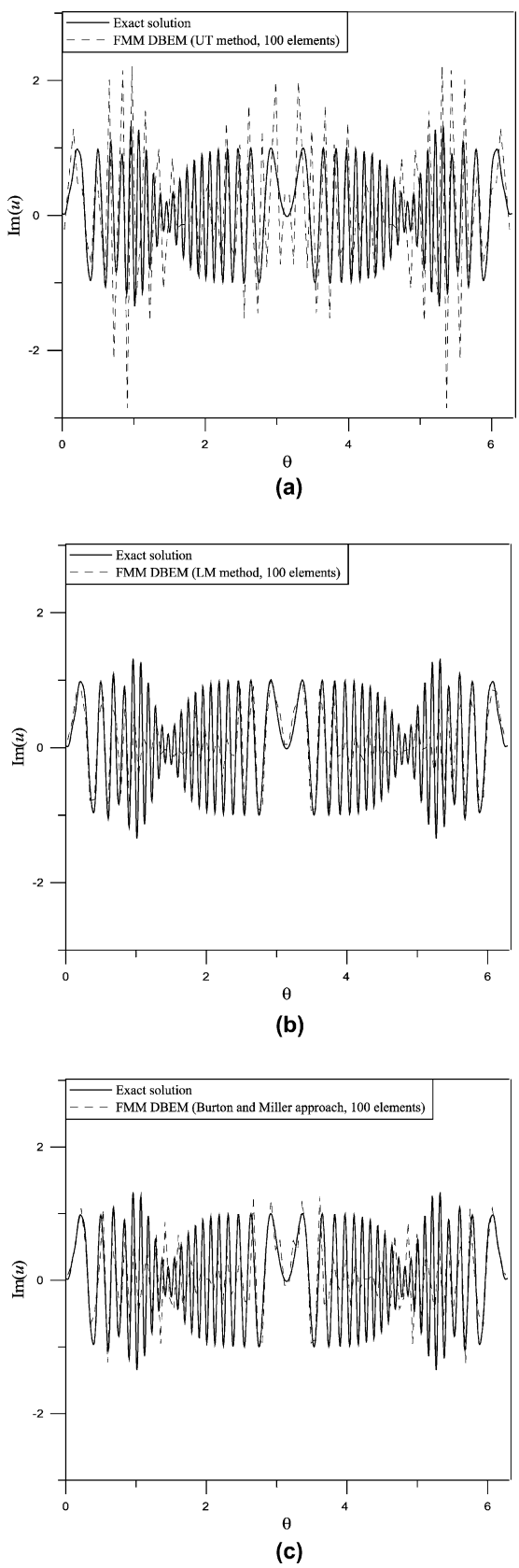

Fig. 7. The boundary solution of scattering field using 100 boundary elements, Im(u), for the case 1. (a) *UT* equation of FMM ($M = 4$), (b) *LM* equation of FMM ($M = 4$), (c) Burton and Miller method of FMM ($M = 4$).

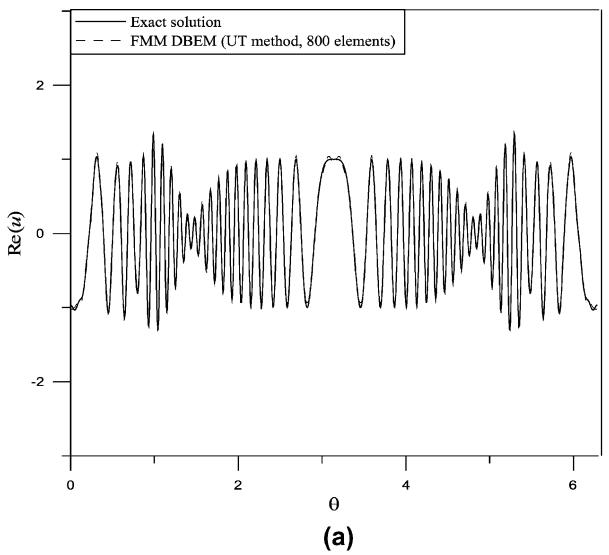

Fig. 8. The boundary solution of scattering field using 800 boundary elements, Re(u), for the case 1. (a) *UT* equation of FMM ($M = 4$), (b) *LM* equation of FMM ($M = 4$), (c) Burton and Miller method of FMM ($M = 4$).

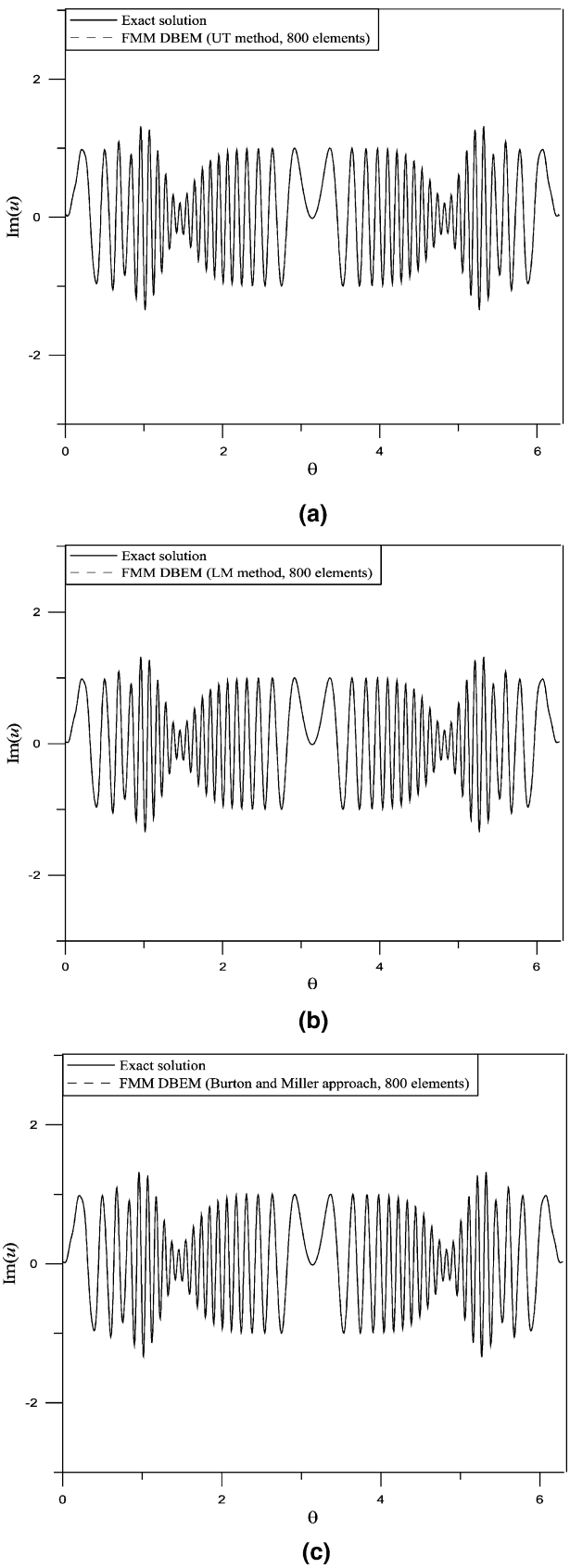

Fig. 9. The boundary solution of scattering field using 800 boundary elements, Im(u), for the case 1. (a) *UT* equation of FMM ($M = 4$), (b) *LM* equation of FMM ($M = 4$), (c) Burton and Miller method of FMM ($M = 4$).

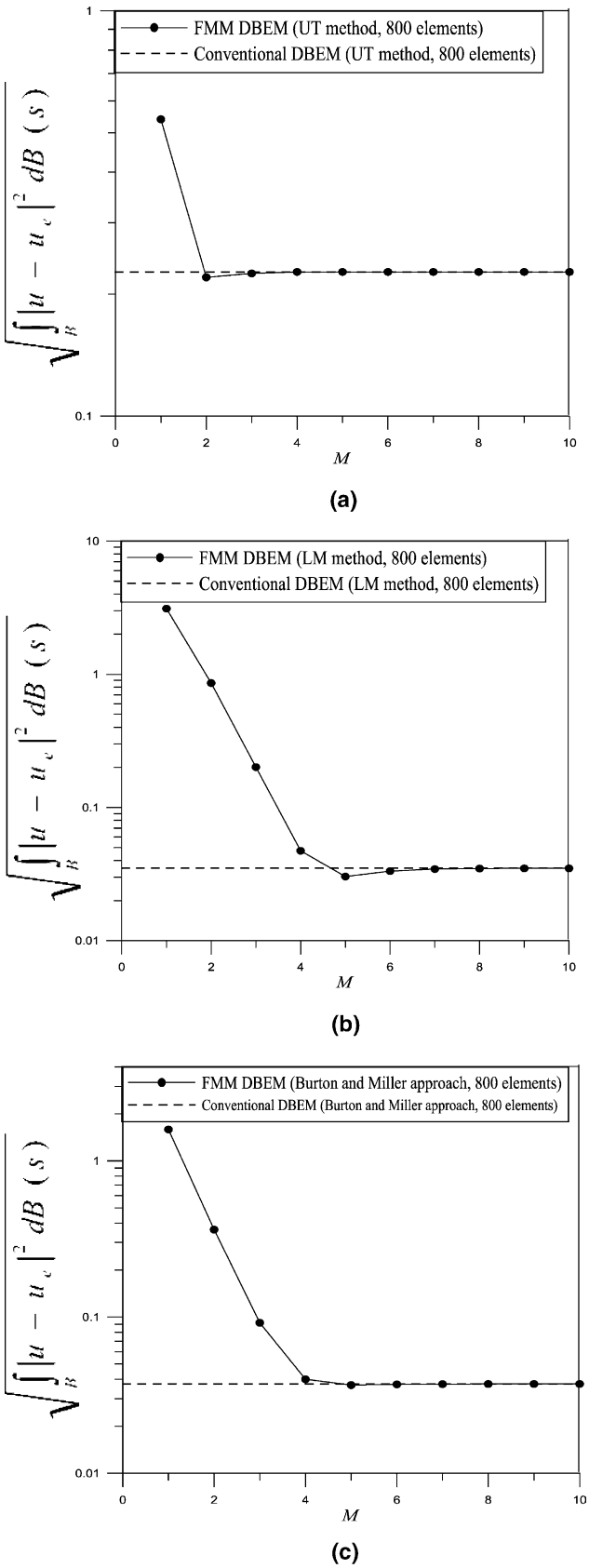

Fig. 10. Comparison of the error norms for the FMM results versus M in the series for the case 1. (a) *UT* equation. (b) *LM* equation. (c) Burton and Miller method.

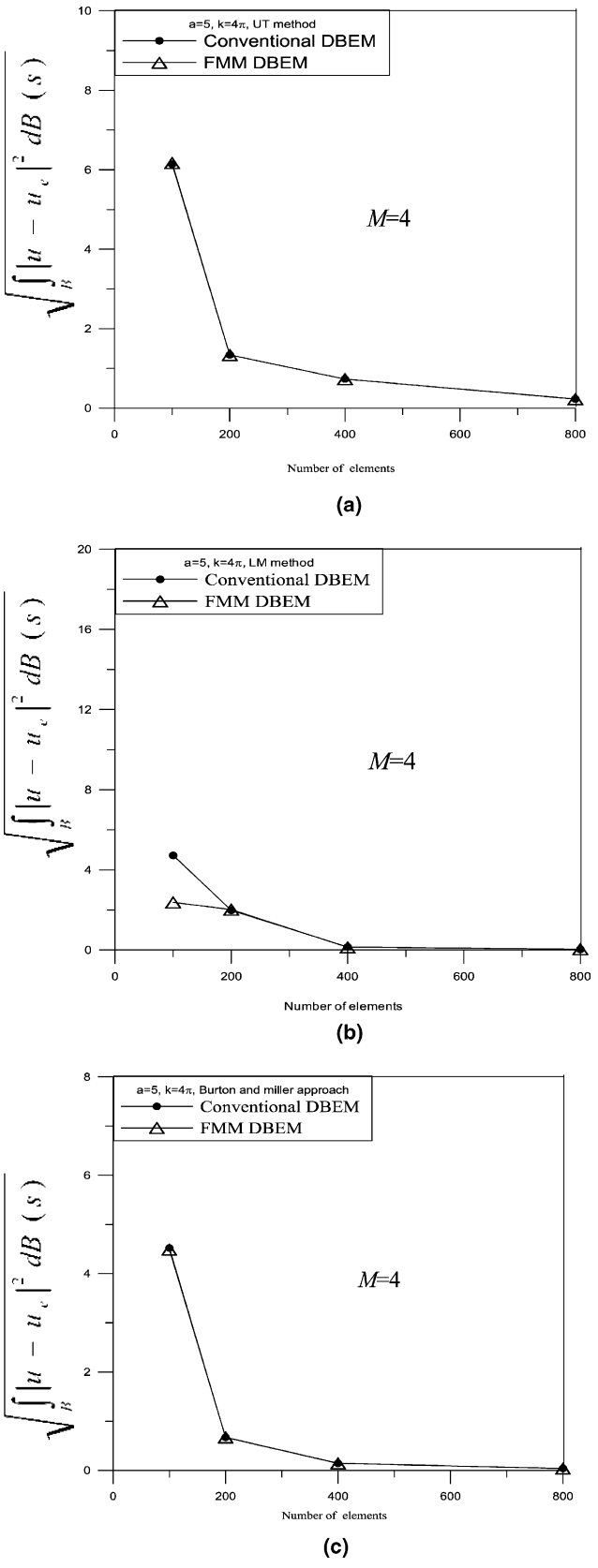

Fig. 11. Comparison of the error norms for the FMM ($M = 4$) and the conventional BEM results versus number of elements for the case 1. (a) *UT* equation, (b) *LM* equation, (c) Burton and Miller method.

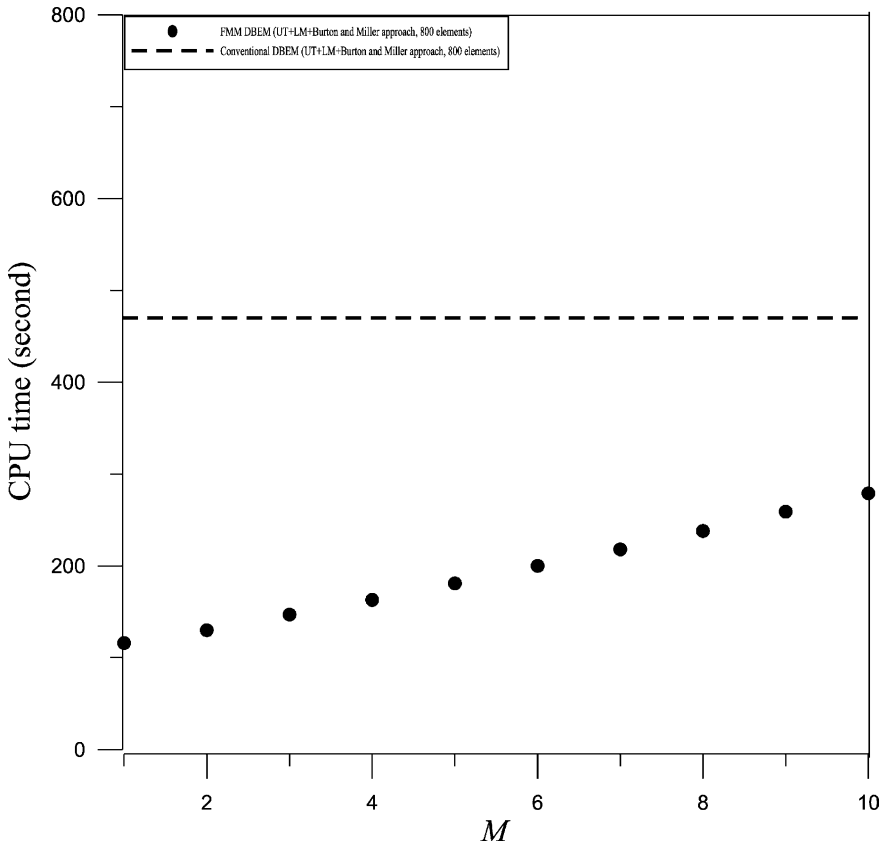

Fig. 12. CPU time by using the FMM versus M in the series for the case 1.

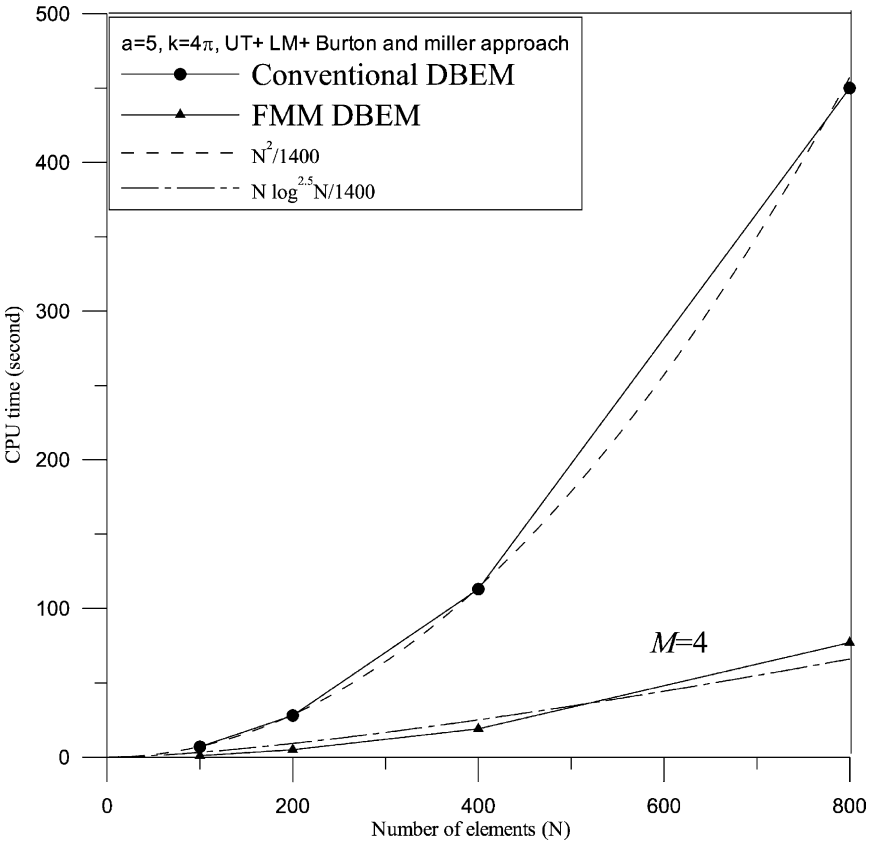

Fig. 13. CPU time by using the FMM ($M = 4$) and the conventional DBEM versus number of elements for the case 1.

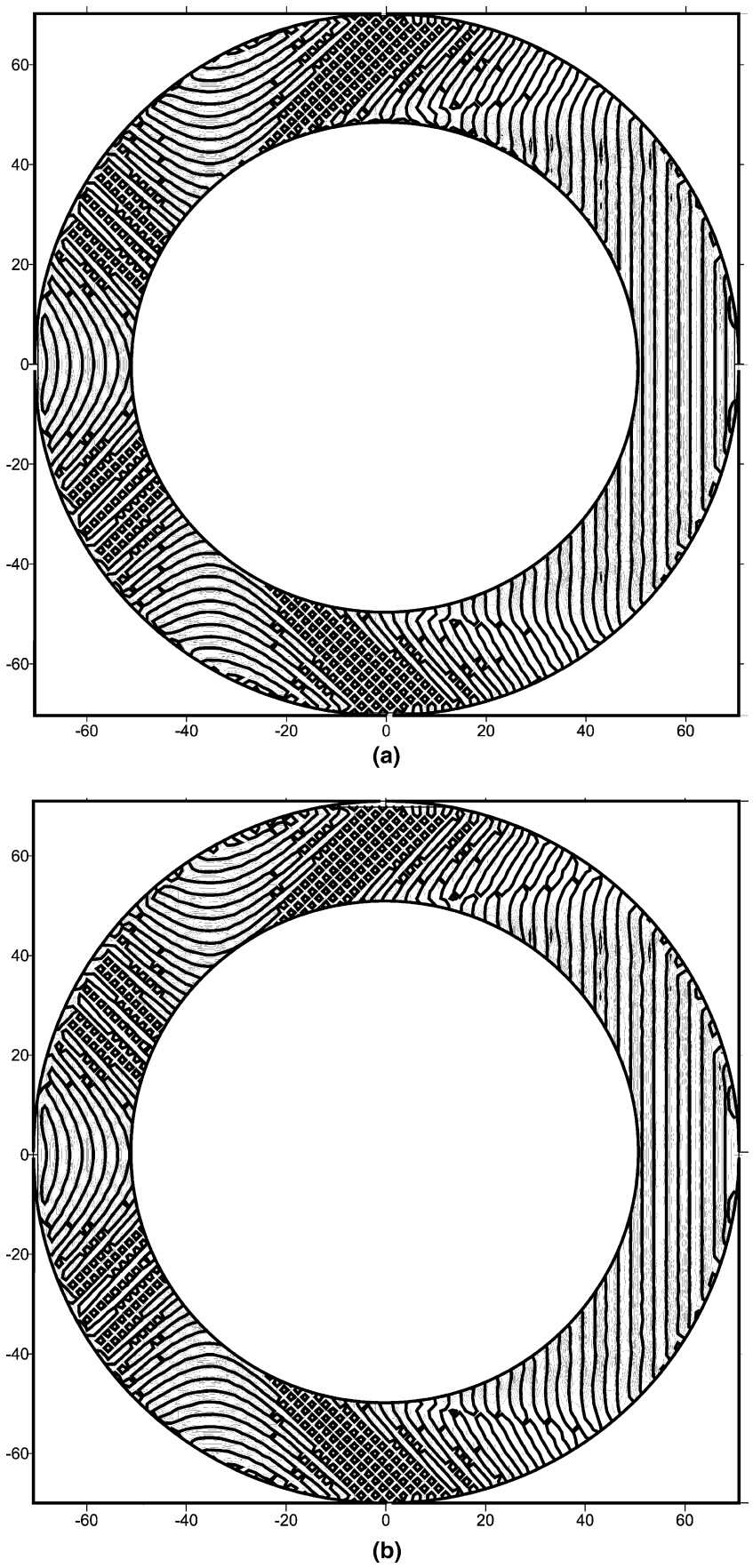

Fig. 14. The contour plot of the real-part solutions in the case 2. (a) Exact solution, (b) FMM results ($M = 3$).

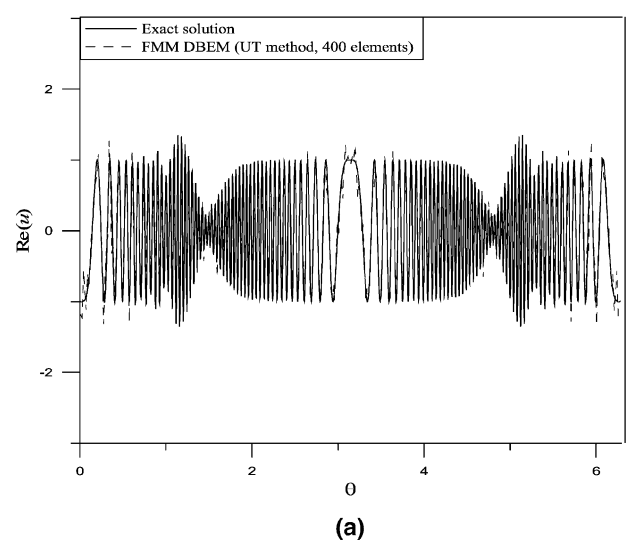

Fig. 15. The boundary solution of scattering field using 400 boundary elements, Re(u), for the case 2. (a) *UT* equation of FMM ($M = 3$), (b) *LM* equation of FMM ($M = 3$), (c) Burton and Miller method of FMM ($M = 3$).

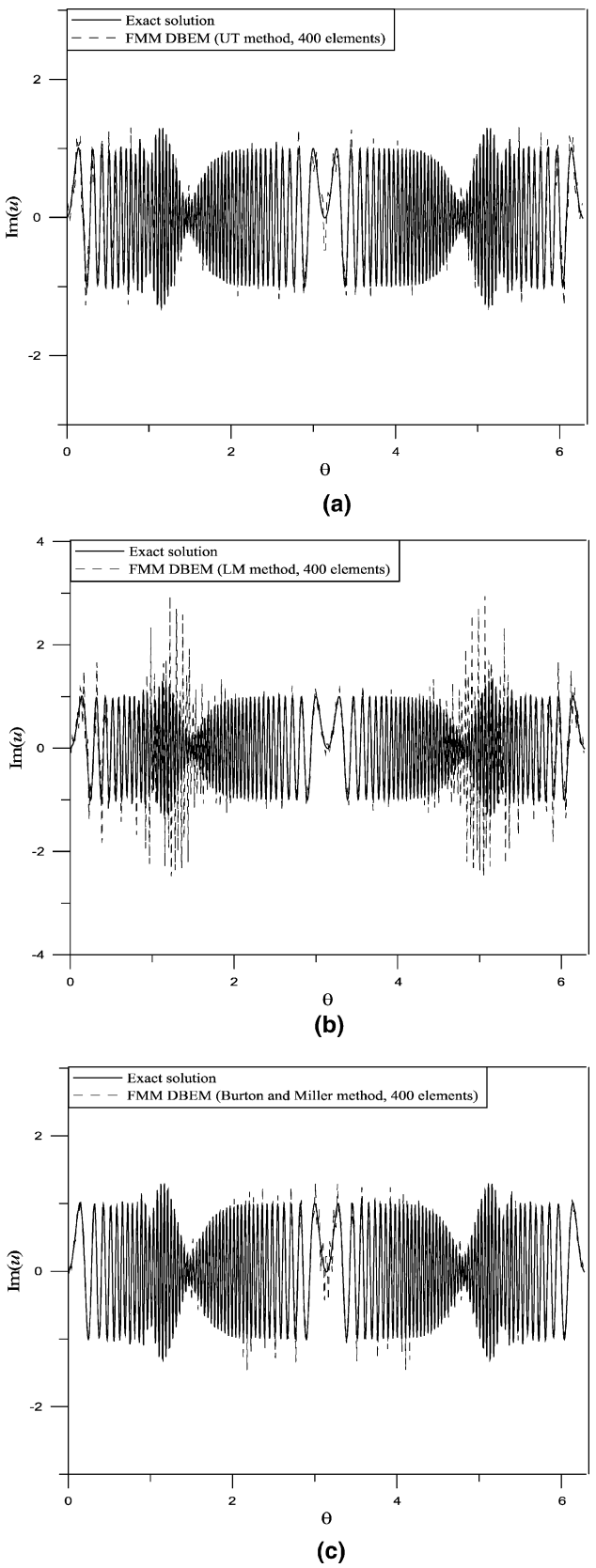

Fig. 16. The boundary solution of scattering field using 400 boundary elements, Im(u), for the case 2. (a) *UT* equation of FMM ($M = 3$), (b) *LM* equation of FMM ($M = 3$), (c) Burton and Miller method of FMM ($M = 3$).

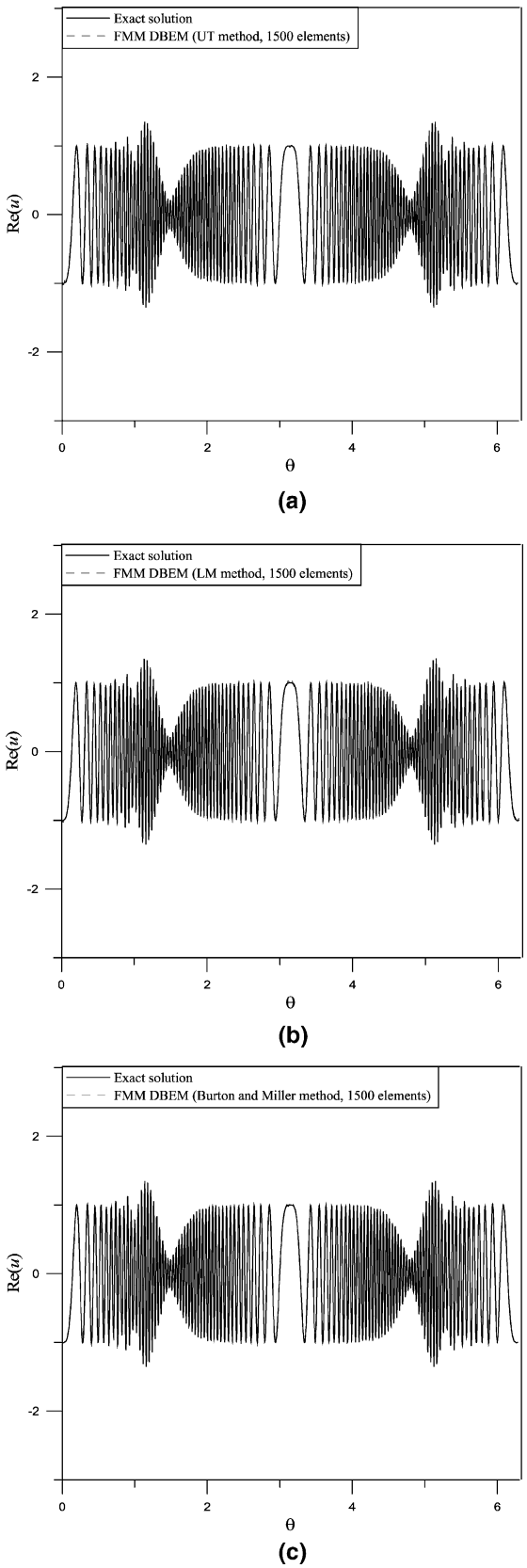

Fig. 17. The boundary solution of scattering field using 1500 boundary elements, Re(u), for case 2. (a) *UT* equation of FMM ($M = 3$), (b) *LM* equation of FMM ($M = 3$), (c) Burton and Miller method of FMM ($M = 3$).

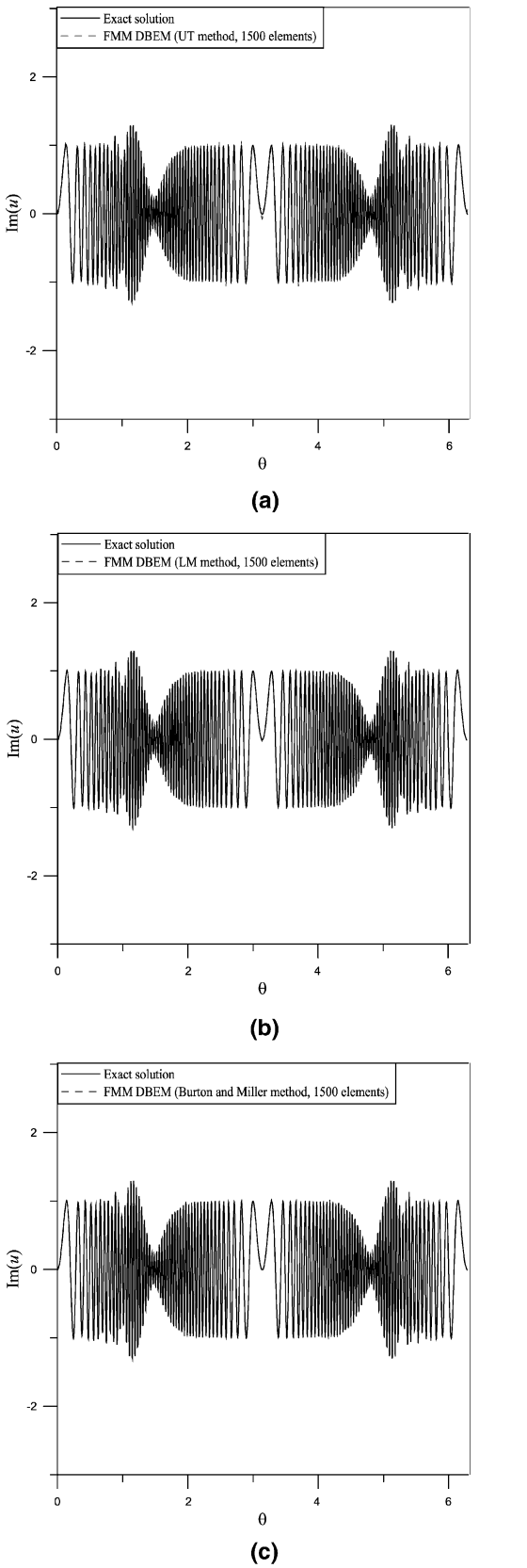

Fig. 18. The boundary solution of scattering field using 1500 boundary elements, Im(u), for the case 2. (a) *UT* equation of FMM ($M = 3$), (b) *LM* equation of FMM ($M = 3$), (c) Burton and Miller method of FMM ($M = 3$).

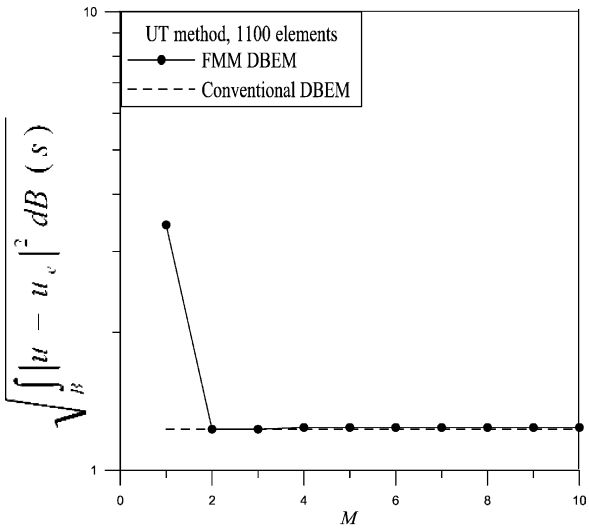

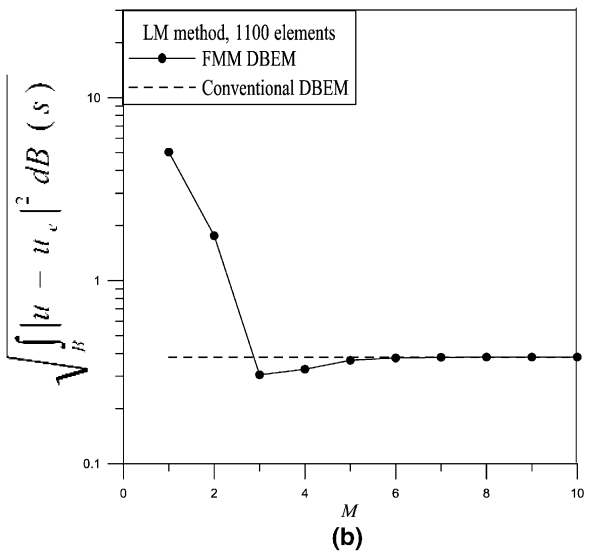

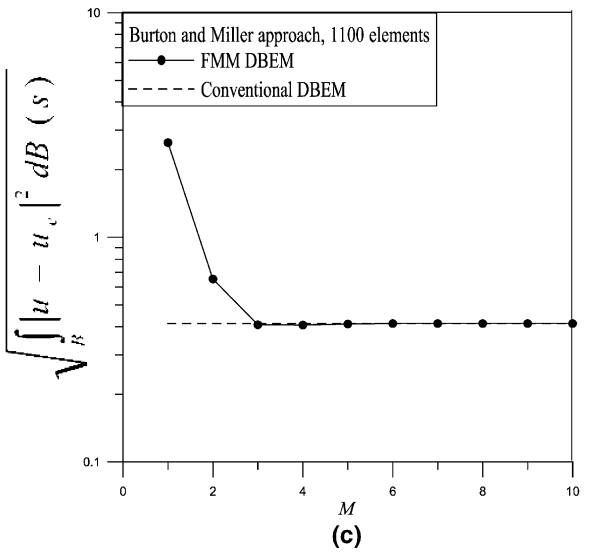

Fig. 19. Comparison of the error norms for the FMM results versus M in the series for the case 2. (a) *UT* equation, (b) *LM* equation, (c) Burton and Miller method.

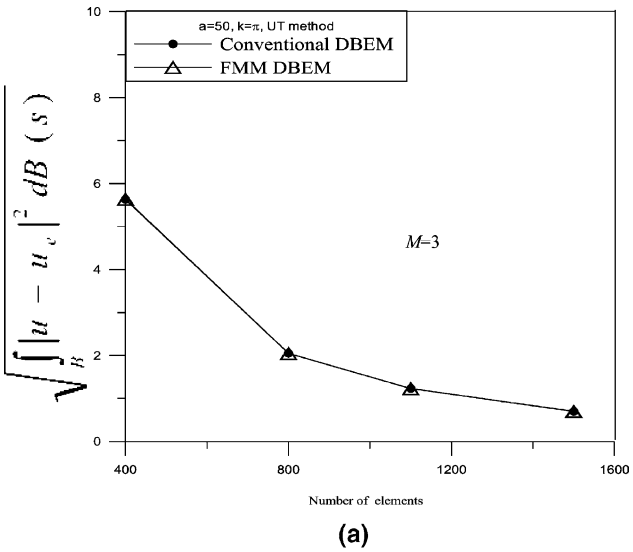

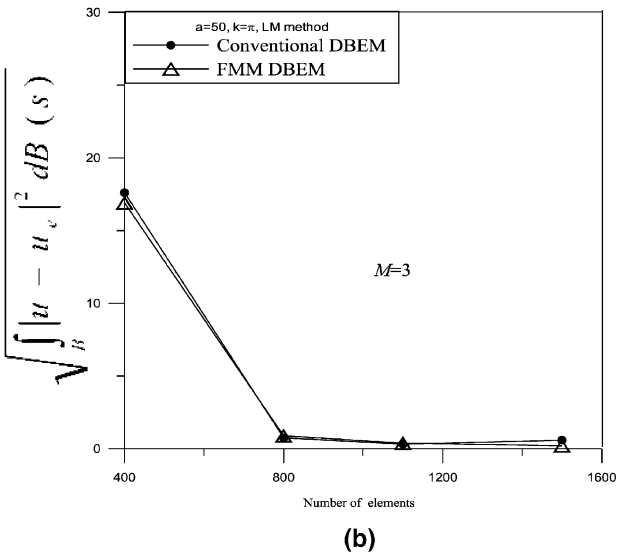

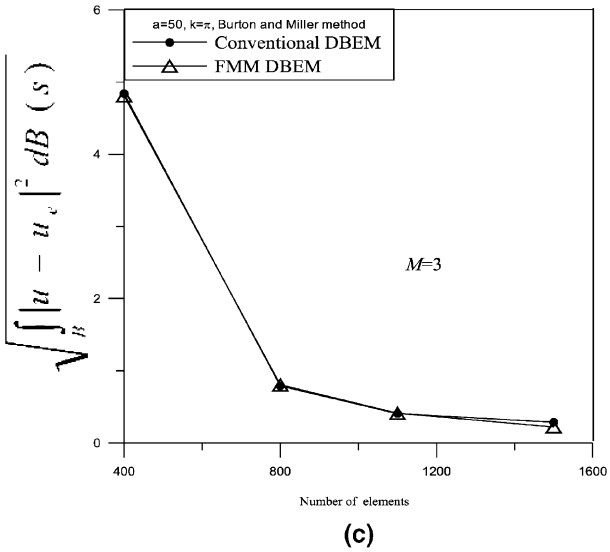

Fig. 20. Comparison of the error norms for the FMM ($M = 3$) and the conventional BEM results versus number of elements for the case 2. (a) *UT* equation, (b) *LM* equation, (c) Burton and Miller method.

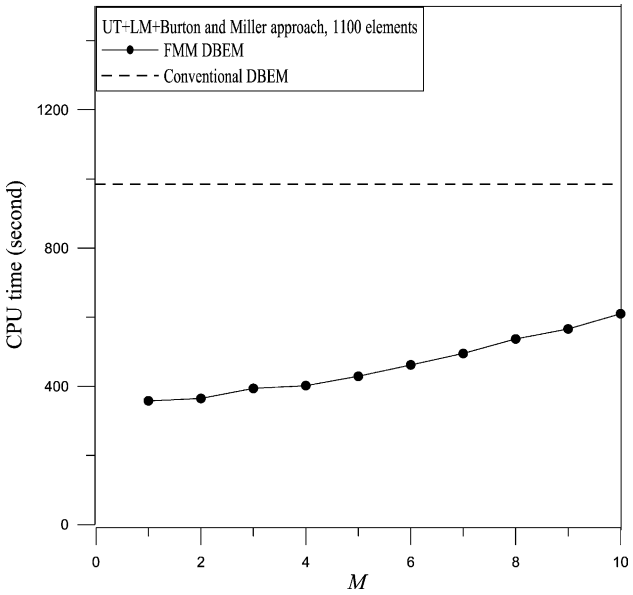

Fig. 21. CPU time by using the FMM versus M in the series for the case 2.

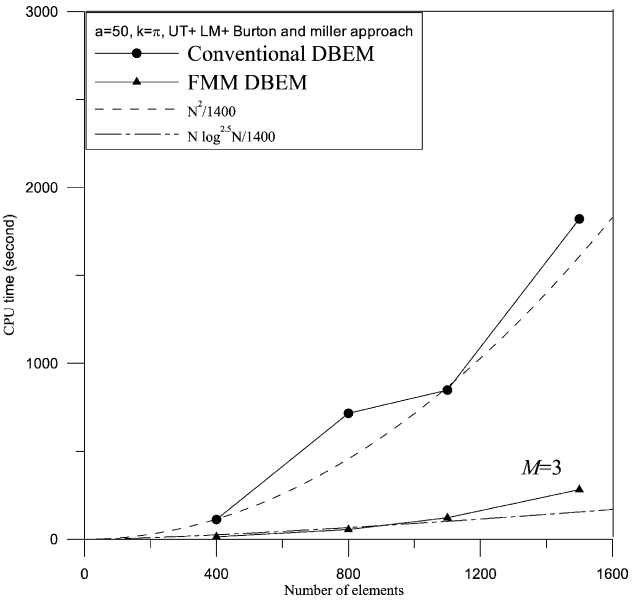

Fig. 22. CPU time by using the FMM ($M = 3$) and the conventional DBEM versus number of elements for the case 2.

a large-scale problem. The same trend of CPU time in comparison with Fig. 13 is observed.

4. Conclusions

In this paper, the four kernels in the dual formulation were expanded into degenerate kernels where the field point and source point were separated. The separable technique promoted the efficiency in determining the influence coefficients. The singular and hypersingular integrals have been transformed into the summability of divergent series and regular integrals. The Burton and Miller formulation by combining the dual boundary integral equations was utilized to solve the exterior acoustic problems for all wave numbers in order to overcome the problem of fictitious frequency. Two illustrative examples have been successfully demonstrated by using the FMM for DBEM formulation in the exterior acoustic problems containing a large-scale scatter. The numerical results were compared well with those of conventional DBEM and analytical solutions. Only a few terms in FMM can reach within the error tolerance. In addition, the CPU time was reduced in comparison with BEM without employing FMM concept.

Acknowledgements

Financial support from the National Science Council, Grant No. NSC-91-2211-E-019-010 and Wu, Ta-You Award for National Taiwan Ocean University to the first author, and the Sinotech Foundation for Research and Development to the second author are gratefully acknowledged.

References

[1] Abramowitz M, Stegun IA. Handbook of mathematical functions with formulation, graphs and mathematical tables. New York: Dover; 1972.
[2] Amini S, Profit ATJ. Analysis of the truncation errors in the fast multipole method for scattering problems. J Comput Appl Math 2000; 115:23–330.
[3] Amini S, Profit ATJ. Analysis of a diagonal form of the fast multipole algorithm for scattering theory. BIT Numer Math 1999;39(4): 585–603.
[4] Amini S. On the choice of the coupling parameter in boundary integral formulation for the exterior acoustic problem. Applic Anal 1990;35: 75–92.
[5] Burton AJ, Miller GF. The application of integral equation methods to numerical solution of some exterior boundary value problems. Proc R Soc Lond, Ser A 1971;323:201–10.
[6] Chen IL, Chen JT, Liang MT. Analytical study and numerical experiments for radiation and scattering problems using the CHIEF method. J Sound Vib 2001;248(5):809–28.
[7] Chen JT, Chen KH, Chen CT. Adaptive boundary element method of time-harmonic exterior acoustic problems in two dimensions. Comput Meth Appl Mech Engng 2002;191:3331–45.
[8] Chen JT, Kuo SR, Lin GH. Analytical study and numerical experiments for degenerate scale problems in the boundary element method for two-dimensional elasticity. Int J Numer Meth Engng 2002;54:1669–81.
[9] Chen JT, Lin JH, Kuo SR, Chiu YP. Analytical study and numerical experiments for degenerate scale problems in boundary element method using degenerate kernels and circulants. Engng Anal Bound Elem 2001;25(9):819–28.
[10] Chen JT, Chen CT, Chen KH, Chen IL. On fictitious frequencies using dual BEM for nouniform radiation problems of a cylinder. Mech Res Commun 2000;27(6):685–90.
[11] Chen JT, Liang MT, Chen IL, Chyuan SW, Chen KH. Dual boundary element analysis of wave scattering from singularities. Wave Motion 1999;30:367–81.

[12] Chen JT, Kuo SR, Chen KH. A nonsingular formulation for the Helmholtz eigenproblems of a circular domain. J Chin Inst Engng 1999;22(6):729–39.
[13] Chen JT. Recent development of dual BEM in acoustic problems. In: Onate E, Idelsohn SR, editors. Keynote lecture. Proceedings of the Fourth World Congress on Computational Mechanics, Argentina, 106.; 1998.
[14] Chen JT, Chen KH. Dual integral formulation for determining the acoustic modes of a two-dimensional cavity with a degenerate boundary. Engng Anal Bound Elem 1998;21(2):105–16.
[15] Chen JT, Hong H-K. Dual boundary integral equations at a corner using contour approach around singularity. Adv Engng Software 1994;21(3):169–78.
[16] Chen JT, Hong H-K. Boundary element method, 2nd ed. Taipei: New World Press; 1992. in Chinese.
[17] Chen YH, Chew WC, Zeroug S. Fast multipole method as an efficient solver for 2D elastic wave surface integral equations. Comput Mech 1997;20:495–506.
[18] Cremers L, Fyfe KR, Sas P. A variable order infinite element for multi-domain boundary element modelling of acoustic radiation and scattering. Appl Acoust 2000;59(3):185–220.
[19] Gel'fand IM, Shilov GE. Generalized functions. New York: Academic Press; 1964.
[20] Hong H-K, Chen JT. Derivations of integral equations of elasticity. J Engng Mech (ASCE) 1988;114(6):1028–44.
[21] Harari I, Barbone PE, Slavutin M, Shalom R. Boundary infinite elements for the Helmholtz equation in exterior domains. Int J Numer Meth Engng 1998;41:1105–31.
[22] Harari I, Hughes TJR. A cost comparison of boundary element and finite element methods for problems of time-harmonic structural acoustics. Comput Meth Appl Mech Engng 1992;97: 77–102.
[23] Harari I, Barbone PE, Montgomery JM. Finite element formulations for exterior problems: application to hybrid methods, non-reflecting boundary conditions and infinite elements. Int J Numer Meth Engng 1997;40:2791–805.
[24] Liang MT, Chen JT, Yang SS. Error estimation for boundary element method. Engng Anal Bound Elem 1999;23:257–65.
[25] Martin O, Laszlo H, Steffen M. Analysis of interior and exterior sound fields using iterative boundary element solvers. J Acoust Soc Am 2001;110(5):2719–69.
[26] Mckenney A. An adaptation of the fast multipole method for evaluating layer potentials in two dimensions. Comput Math Applic 1996;31(1):33–57.
[27] Michel AT, Noureddine A. Efficient evaluation of the acoustic radiation using multipole expansion. Int J Numer Meth Engng 1999;46:825–37.
[28] Michel AT, Noureddine A. A novel acceleration method for the variational boundary element approach based on multipole expansion. Int J Numer Meth Engng 1998;42:1199–214.
[29] Nishimura N, Yoshida K-I, Kobayashi S. A fast multipole boundary integral equation method for crack problems in 3D. Engng Anal Bound Elem 1999;23:97–105.
[30] Nishimura N. Fast multipole accelerated boundary integral equation methods. Appl Mech Rev 2002;55(4):1–27.
[31] Rehr JJ, Albers RC. Scattering-matrix formulation of curved-wave multiple-scattering theory: application to X-ray-absorption fine structure. Am Phys Soc 1990;41(12):8139–49.
[32] Ricardo EM. The multipole expansion: a new look. J Sound Vib 2000; 236(5):904–11.
[33] Rokhlin V. Rapid solution of integral equations of scattering theory in two dimensions. J Comput Phys 1990;86:414–39.
[34] Rokhlin V. Rapid solution of classical potential theory. J Comput Phys 1983;60:187–207.
[35] Stewart JR, Hughes TJR. *h*-Adaptive finite element computation of time-harmonic exterior acoustics problems in two dimension. Comput Meth Appl Mech Engng 1997;146:65–89.
[36] Takahashi T, Kobayashi S, Nishimura N. Fast multipole BEM simulation of overcoring in an improved conical-end borehole strain measurement method. Mechanics and engineering. Beijing, China: Tsinghua University Press; 1999. p. 120–127, In Honor of Professor Qinghua Du's 80th Anniversary.
[37] Yoshida K-I, Nishimura N, Kobayashi S. Application of fast multipole Galerkin boundary integral equation method to crack problems in 3D. Int J Numer Meth Engng 2001;50:525–47.
[38] Young DL, Tsai CC, Eldho TI. Solution of Stokes flow using an iterative DRBEM based on compactly-supported, positive-definite radial basis function. Comput Math Applic 2002;43:607–19.